

Thomas LaGrange
Senior Staff Scientist



Lorentz Transmission
Electron Microscopy: Theory,
Practice, Simulations, and
Quantitative Phase
reconstruction

Doctoral Course MSE-670

November 16th, 2022

Outline:

Lorentz microscopy has been used extensively for the past 40 years to study magnetic domain structure and magnetization reversal mechanisms in magnetic thin films and elements. Here, a brief introduction to standard image modes in TEM and the theory involved is presented. The second half of lectures is devoted to discussing how the sample's phase shift and magnetic properties can be quantified from the LTEM observations.

- 1) Lorentz Transmission Electron Microscopy (LTEM)
 - A. Lorentz Force
 - B. LTEM Imaging modes
 - C. Examples
- 2) Simulation and quantitative analysis
 - A. Modeling magnetic images in a real microscope
 - B. Transport of Intensity Equations (TIE)
 - C. Examples

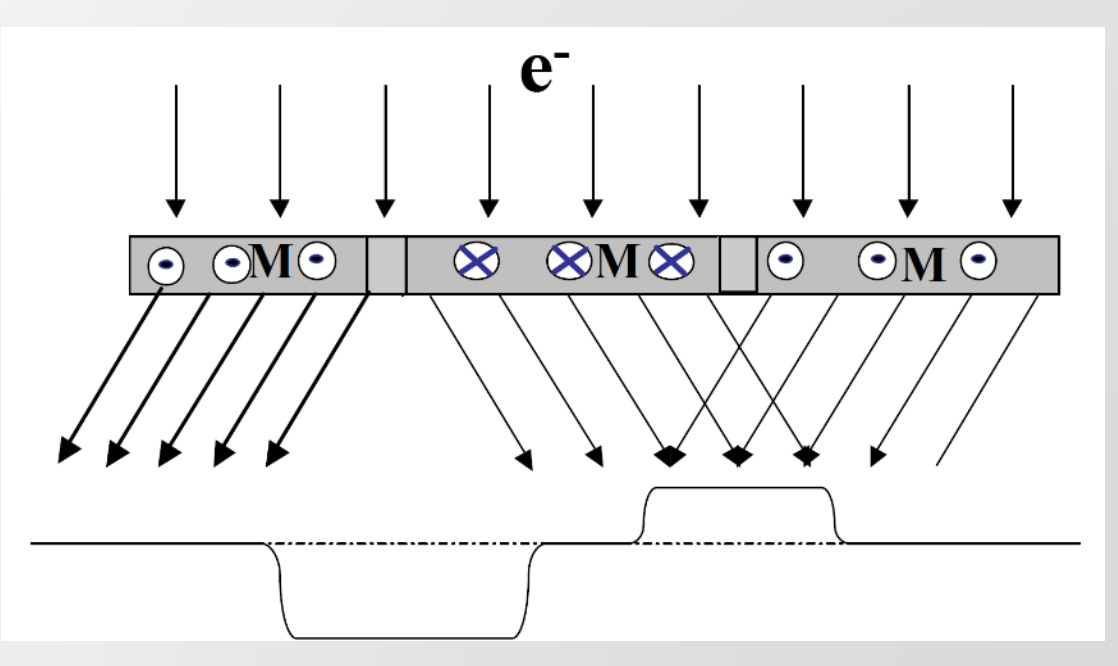
Lorentz TEM (LTEM): Lorentz force

Electrons, which pass a region having electrostatic and/or magnetic fields, are deflected by Lorentz force F_L

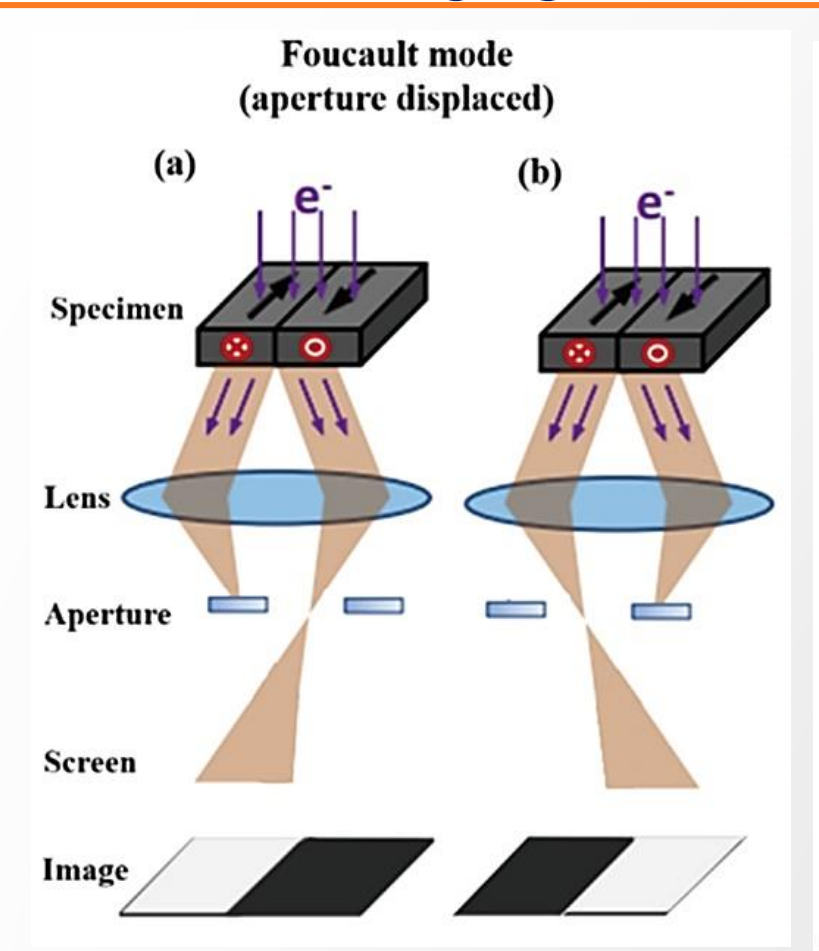
$$F_L = -e(E + \nu \times \vec{B})$$

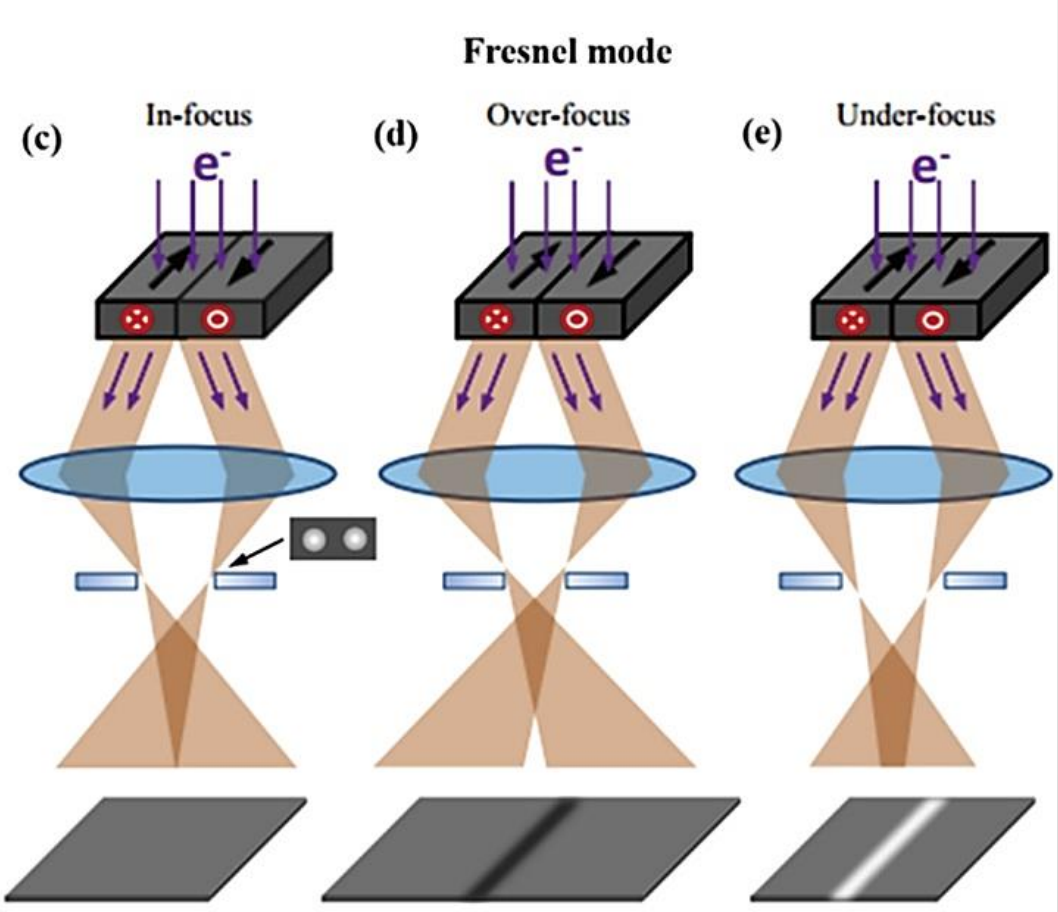
Suppose $E \approx 0$, and F_L acts normal and deflects the electron beam. Only the in-plane magnetic induction, B_{\perp} , deflects the beam.

$$\vec{B} = \vec{B}_{\perp} + B_z \vec{n}$$



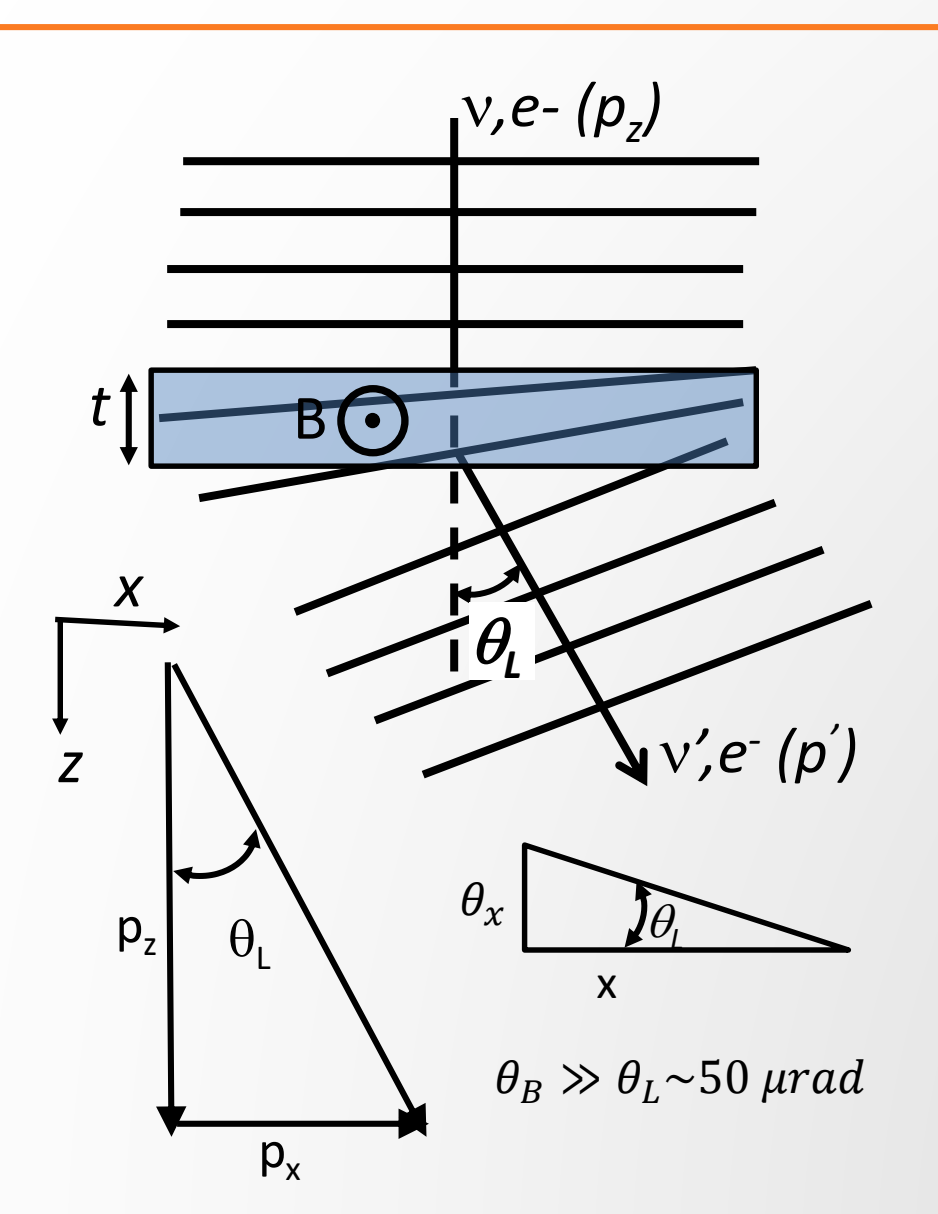
LTEM: Lorentz Transmission Electron Microscopy Different imaging modes for observing magnetic features





In-focus observation Scattering contrast that distinguishes domains Out-of-focus observation
Interference contrast that distinguishes the intersection between domains or changing spin states

Diffraction due to sample magnetization



$$p_{x} = \int_{0}^{\tau} \overrightarrow{F_{L}} d\tau = e \int_{o}^{t} B_{\perp} dz = eB_{\perp} t$$
$$p_{z} = mv$$

Lorentz deflection gives small angles

$$\theta_L \approx \frac{p_x}{p_z} = \frac{eB_\perp t}{h\vec{k}} = \frac{eB_\perp t}{mv} = C_E B_\perp t$$

$$\varphi(x) = -2\pi \vec{k}\theta_x = -\frac{2\pi e B_\perp t x}{h}$$

For a varying \overrightarrow{B} , we arrive at the general solution for the phase shift due to a magnetic induction within the sample

$$\varphi (x,y) = -\frac{2\pi e}{h} \int \overrightarrow{B} ds$$

Measuring the Lorentz diffraction angle θ_L with small angle diffraction experiments

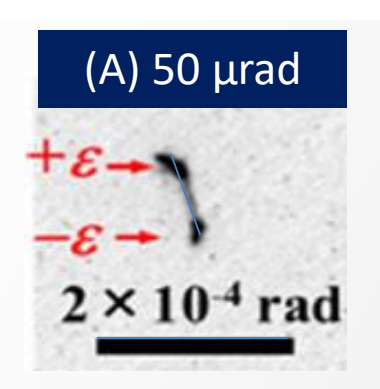
PHYSICAL REVIEW B 94, 024407 (2016)

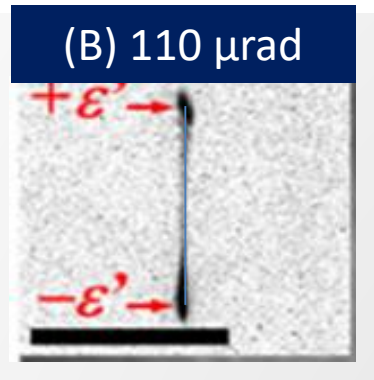
Lorentz microscopy and small-angle electron diffraction study of magnetic textures in $La_{1-x}Sr_xMnO_3$ (0.15 < x < 0.30): The role of magnetic anisotropy

A. Kotani, H. Nakajima, K. Harada, L. Y. Ishii, and S. Mori L.

Department of Materials Science, Osaka Prefecture University, Sakai, Osaka 599-8531, Japan

Center for Emergent Material Science, the Institute of Physical and Chemical Research (RIKEN), Hatoyama, Saitama 350-0395, Japan (Received 21 December 2015; revised manuscript received 15 June 2016; published 6 July 2016)



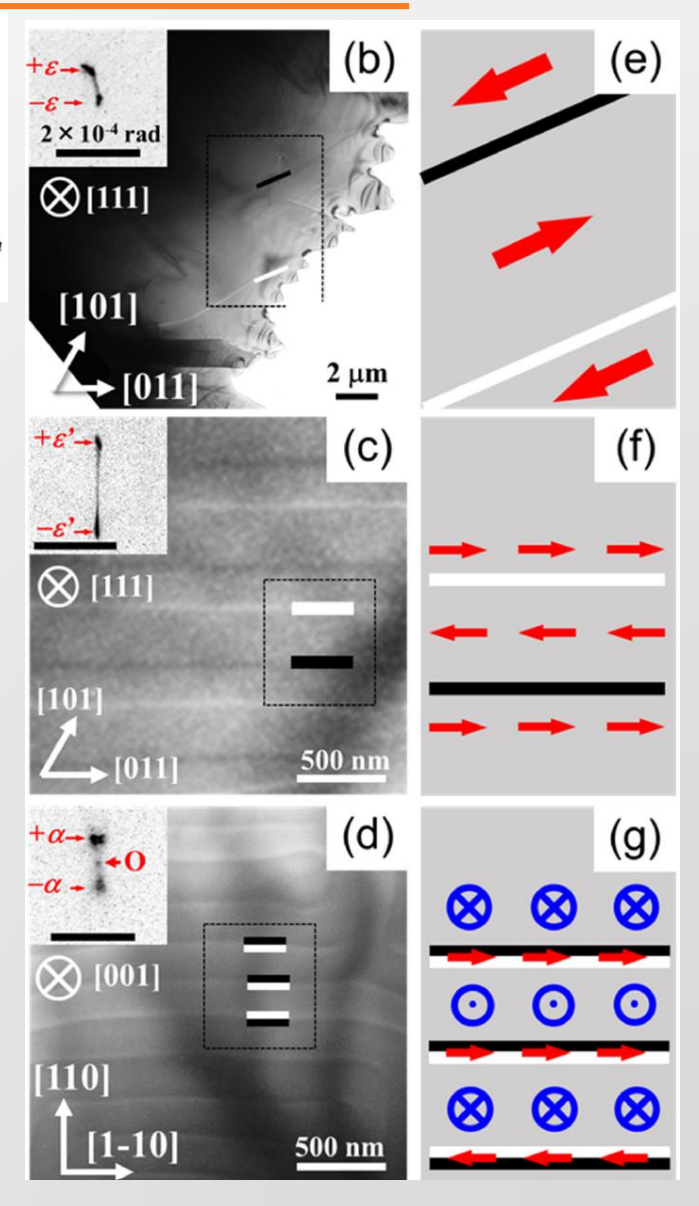


$$\theta_L = \frac{eB_{\perp}t}{mv} = C_E B_{\perp}t$$

$$C_E = \frac{9.37783}{\sqrt{E_o + 0.97485 \times 10^{-3} E_o^2}} \xrightarrow{200 \text{ kV}} 0.607 \text{ } \mu \text{rad/T/nm}$$

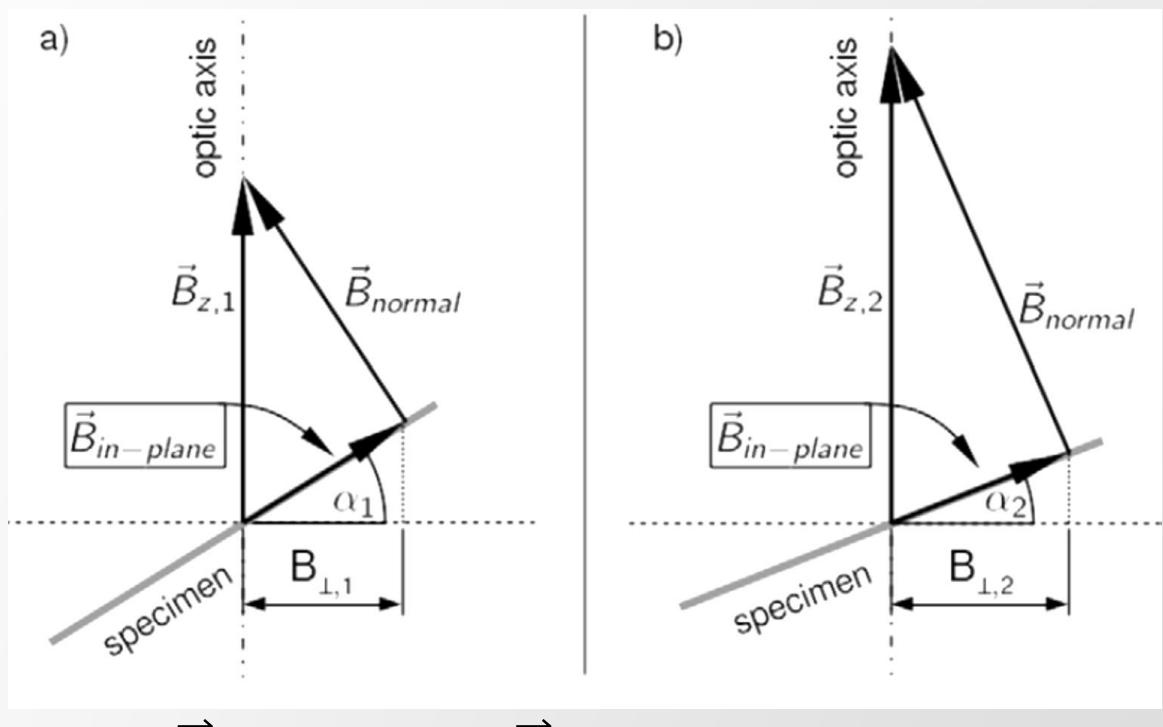
For a TEM foil thickness of 150 nm

(A)
$$B_{\perp} = 550 \text{mT}$$
 (B) $B_{\perp} = 1.2 \text{ T}$



Lorentz TEM (LTEM): Lorentz force

The components of the magnetic induction in the sample can be determined by tilting the specimen.

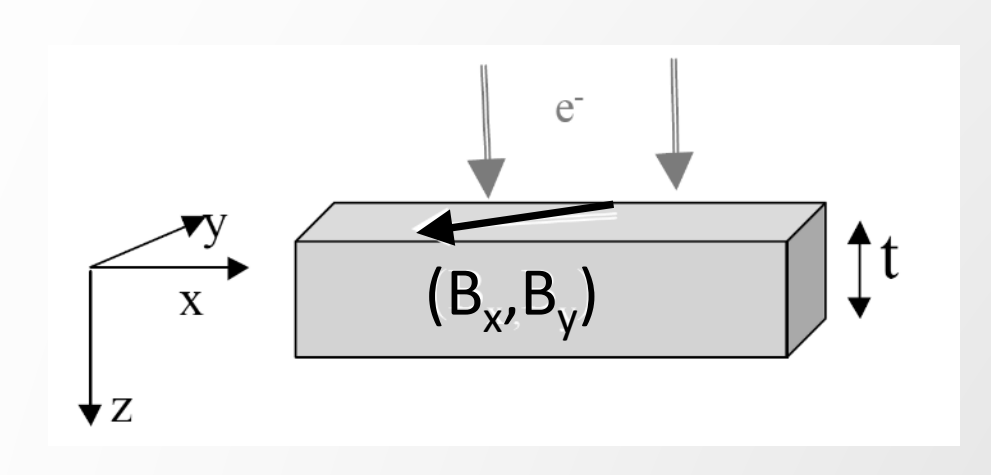


$$\vec{B}_{in-plane} = \vec{B}_{\perp} + B_z \sin \alpha$$

$$\frac{B_{\perp,1}}{B_{\perp,2}} = \frac{\sin \alpha_1}{\sin \alpha_2}$$

Determining the 3 components of the magnetic induction vector in the sample

A Sample of thickness (t) having internal magnetic fields with magnetic inductive vector (\vec{B}_{\perp}) in two direction, B_x and B_y



Gauss's Law

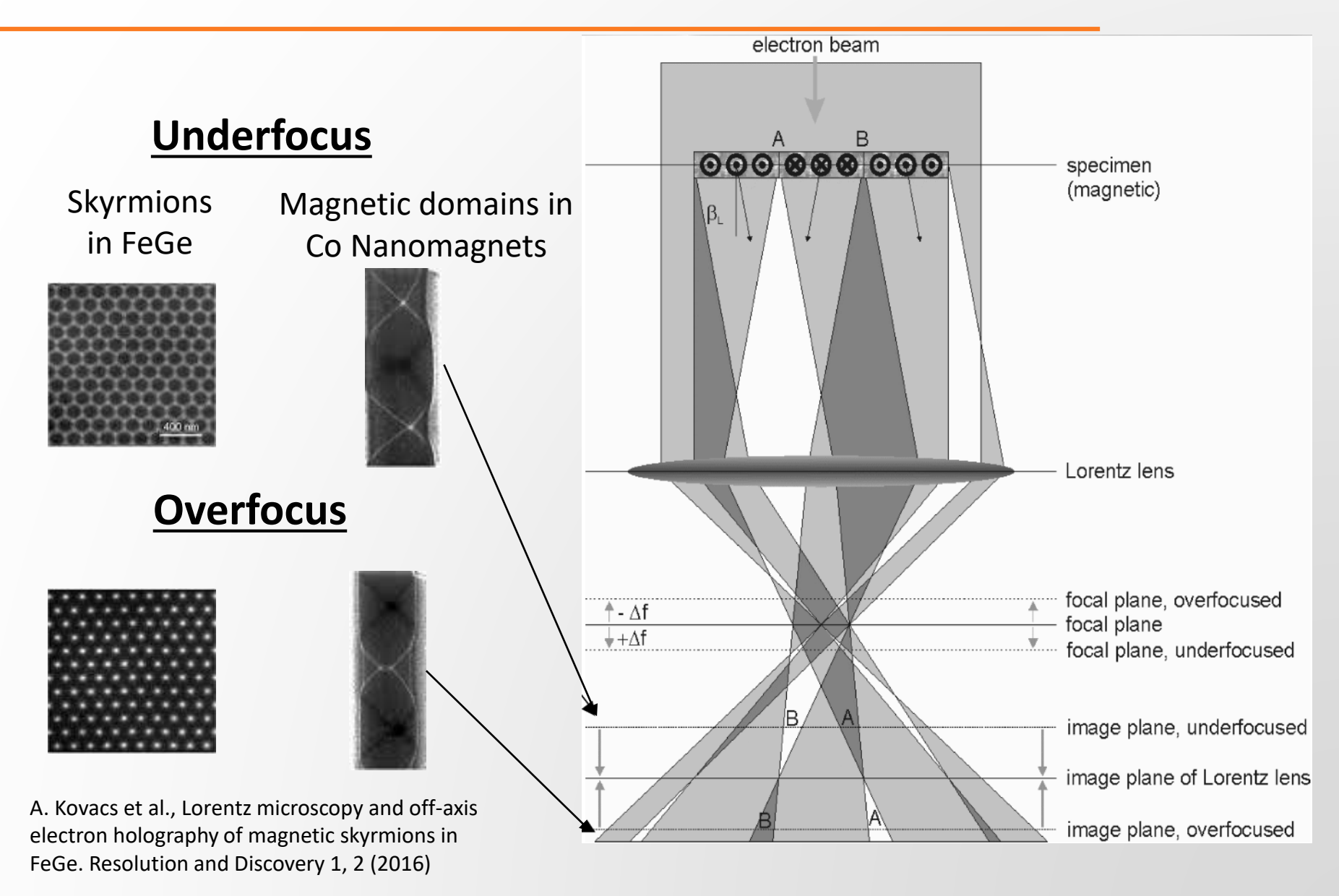
$$Div \vec{B} = 0 \Longrightarrow \frac{\partial B_x}{\partial x} = -\frac{\partial B_y}{\partial y}$$
$$\frac{\partial^2 \Delta \varphi}{\partial x \partial y} = -\frac{2\pi e t}{h} \frac{\partial B_y(x, y)}{\partial y}$$
$$B_x = -\int \frac{\partial B_y}{\partial y} dx = \frac{h}{2\pi e t} \frac{\partial^2 \Delta \varphi}{\partial x \partial y} dx$$

$$B_{x} = \frac{h}{2\pi e t} \frac{\partial \Delta \varphi}{\partial y}$$

and

$$B_y = -\frac{h}{2\pi e t} \frac{\partial \Delta \varphi}{\partial x}$$

LTEM: Fresnel imaging mode



Example: Magnetic domain structure in ferromagnetic SMA



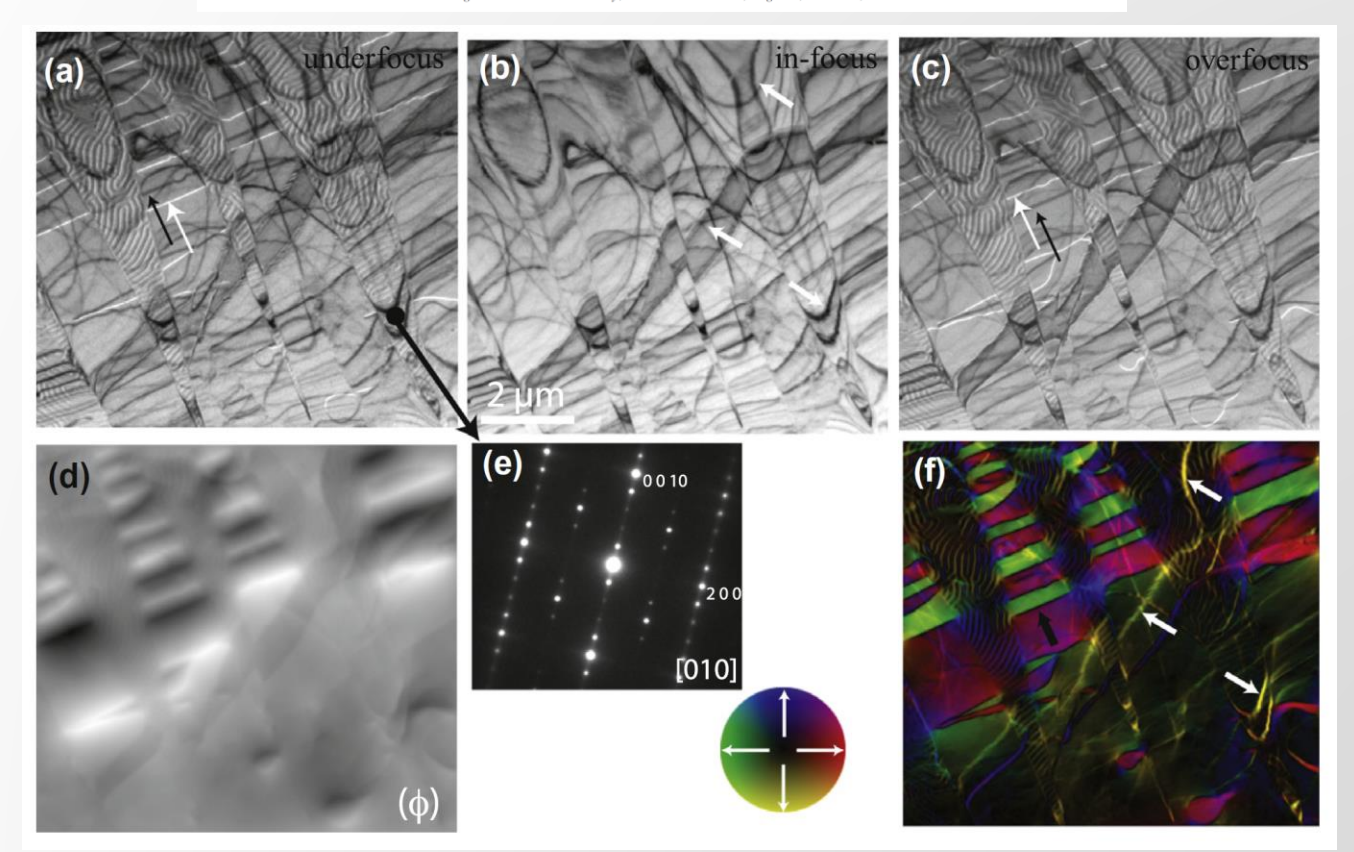




In situ lorentz TEM magnetization study of a Ni–Mn–Ga ferromagnetic shape memory alloy

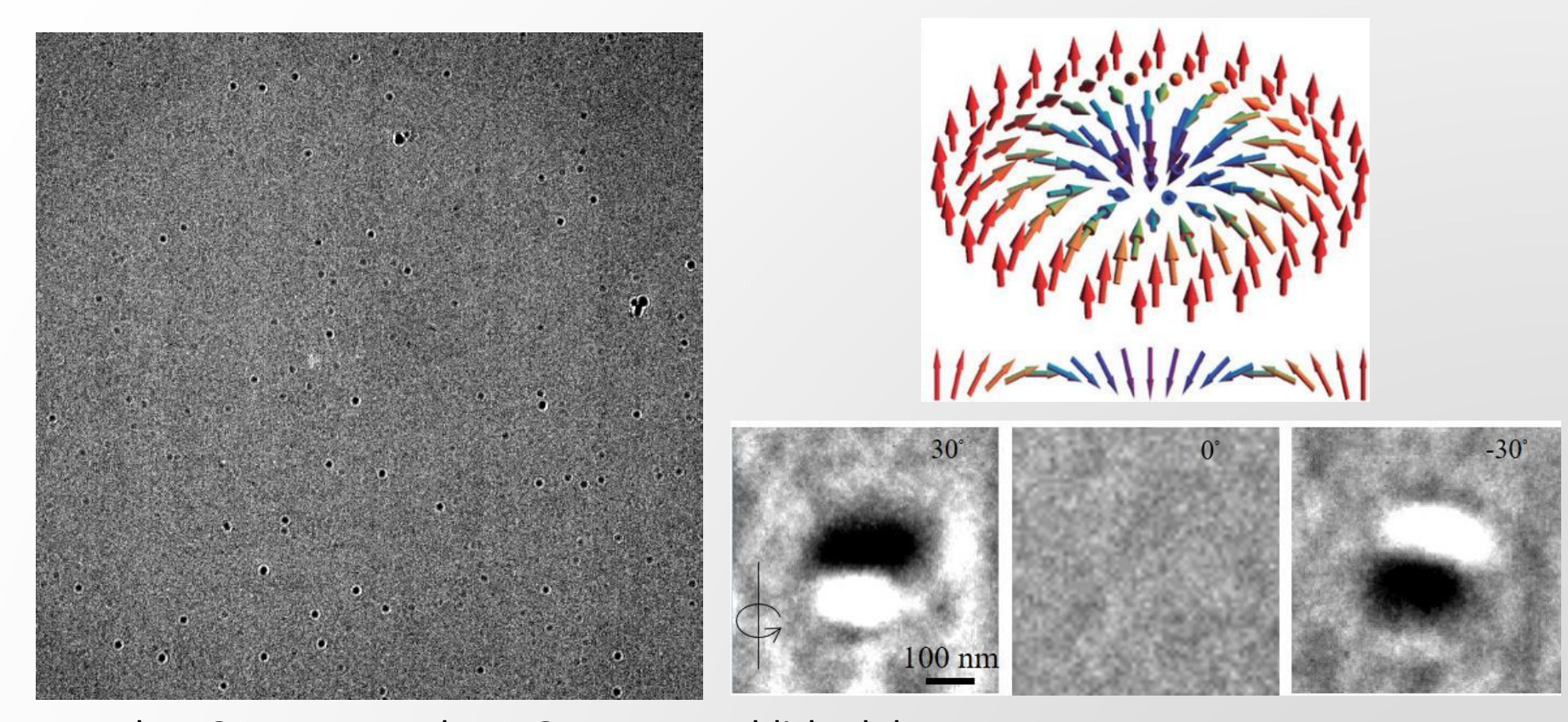
A. Budruk a, C. Phatak b, A.K. Petford-Long b, M. De Graef a,*

^a Department of Materials Science and Engineering, Carnegie Mellon University, Pittsburgh, PA 15213, USA
^b Argonne National Laboratory, 9700 S Cass Avenue, Argonne, IL 60439, USA



thomas.lagrange@epfl.ch • www.epfl.ch • lumes.epfl.ch • +41 (0)21 6935861

Example: In-situ LTEM observations of Nèel type Skyrmions (Pt-Co multilayers) under an applied field (~100 mT)



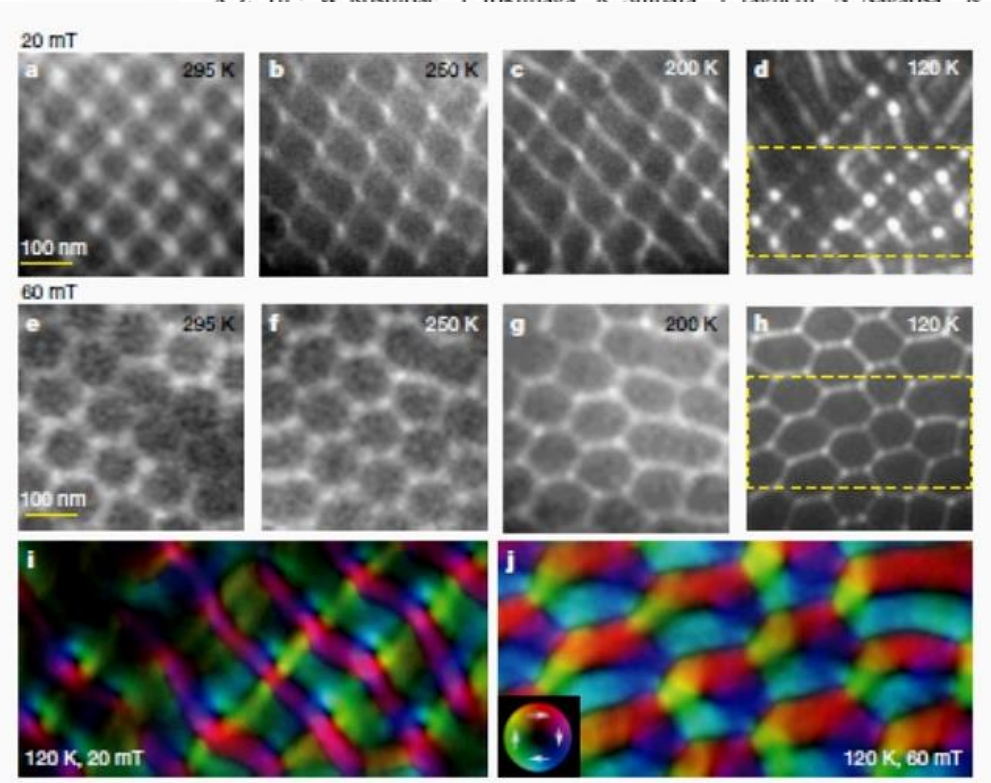
I. Madan, G. Berruto and T. LaGrange Unpublished data

Complementary study in a similar system
Zhang, S., et al. (2018). "Creation of a thermally assisted skyrmion lattice in Pt/Co/Ta multilayer films." Applied Physics Letters **113**(19): 192403.

Example: Imaging Skyrmions in CoZnMn alloys

Transformation between meron and skyrmion topological spin textures in a chiral magnet

X. Z. Vul* W. Koshibae¹, V. Tokunaga², K. Shibata¹, V. Taguchi¹, N. Nagaosa^{1,3} & Y. Tokura^{1,3}



The equilibrium period of the helical phase

$$L_D = 4\pi \frac{A}{D}$$

where A is the micromagnetic exchange constant and D is the DMI constant

Critical field corresponding to the saturation field of the system

$$H_D = \frac{D^2}{2M_s A}$$

where M_s is the magnetization

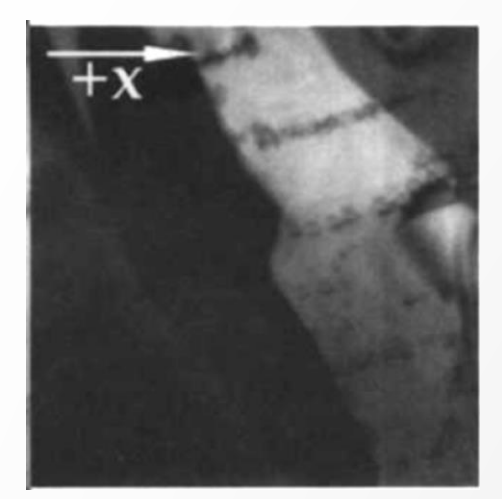
Fig. 3 | Stability of the square (anti)meron and hexagonal skyrmion lattices in the (001) plate of Co₈Zn₉Mn₃, a-h, Over-focused Lorentz TEM images of the square (anti)meron (a-d) and hexagonal skyrmion (e-h) lattices observed with decreasing temperature at a magnetic field of 20 mT and 60 mT, respectively (experimental procedures are denoted by

red dashed arrows in the phase diagram in Extended Data Fig. 3b).

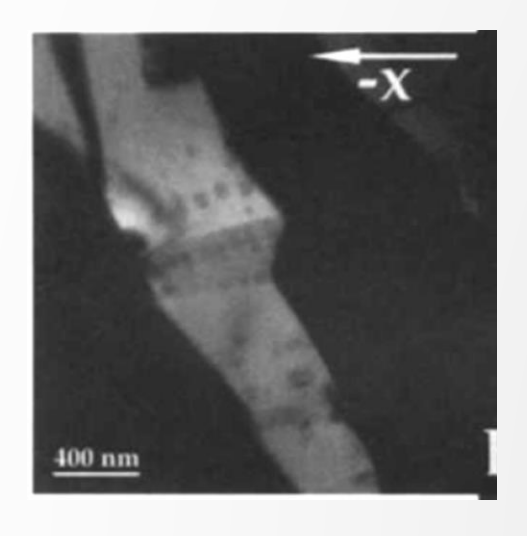
i, j, Magnetization textures for the boxed regions in d and h, respectively, deduced by analysing Lorentz TEM images with the transport-of-intensity equation. The colour wheel in the inset of j indicates the in-plane magnetization direction.

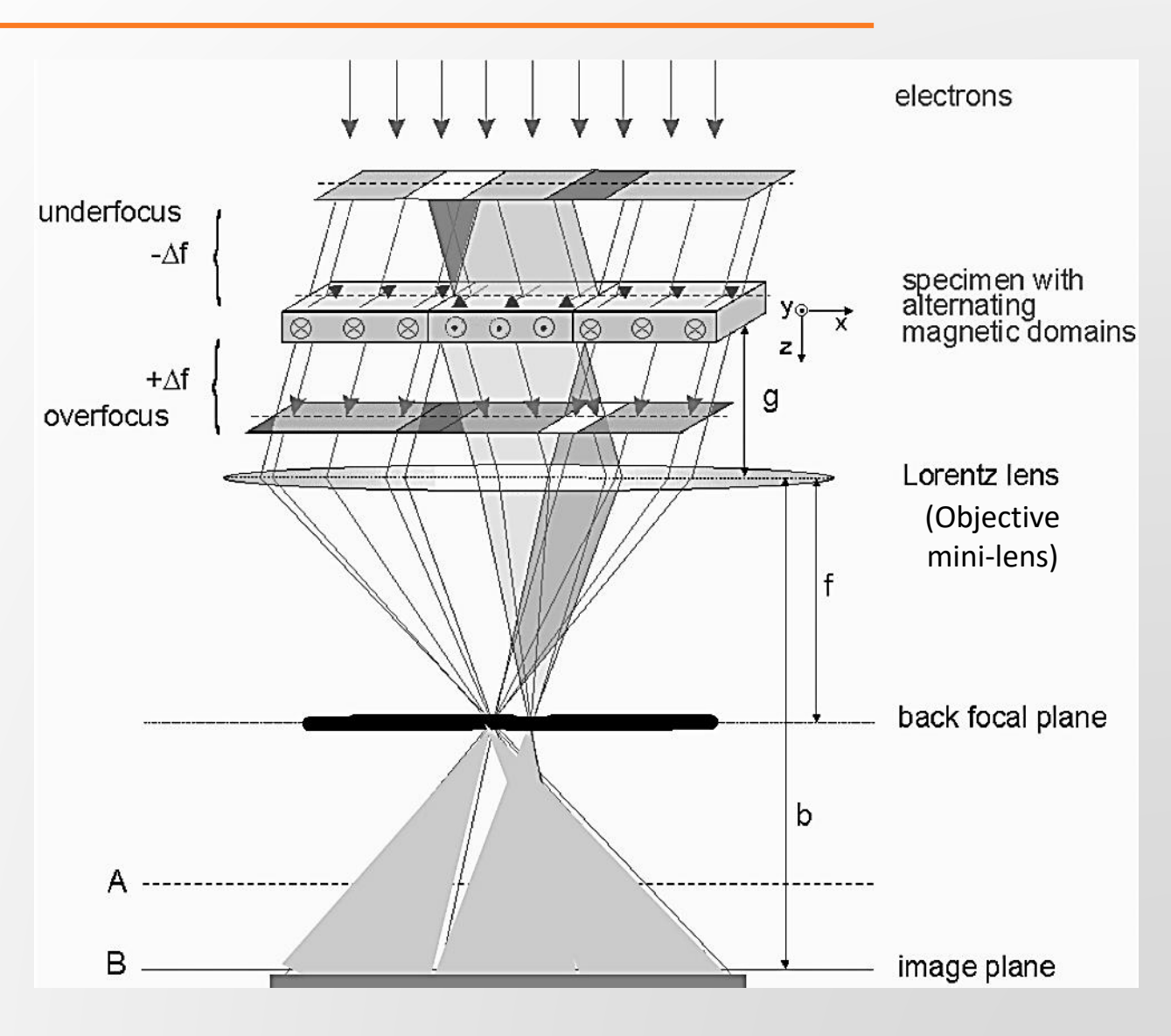
LTEM: Foucault imaging

Aperture displaced $2\theta_L$

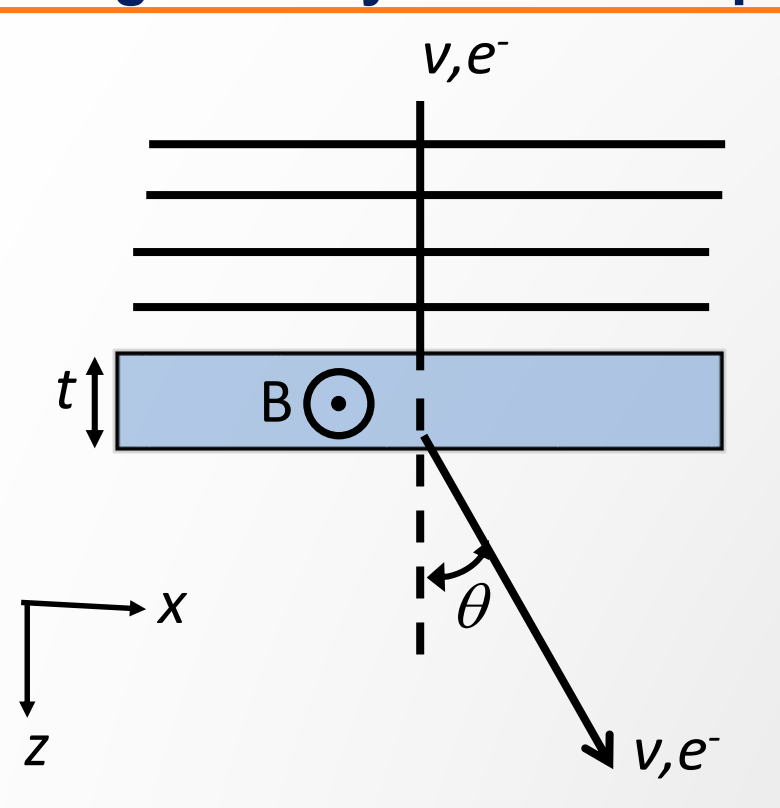


Aperture displaced $-2\theta_1$

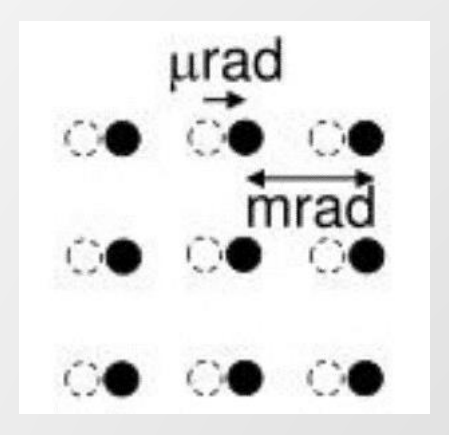




Foucualt imaging is darkfield image formed using the magnetically deflected spots



The Foucault image is a darkfield image formed by the magnetically scattered beams



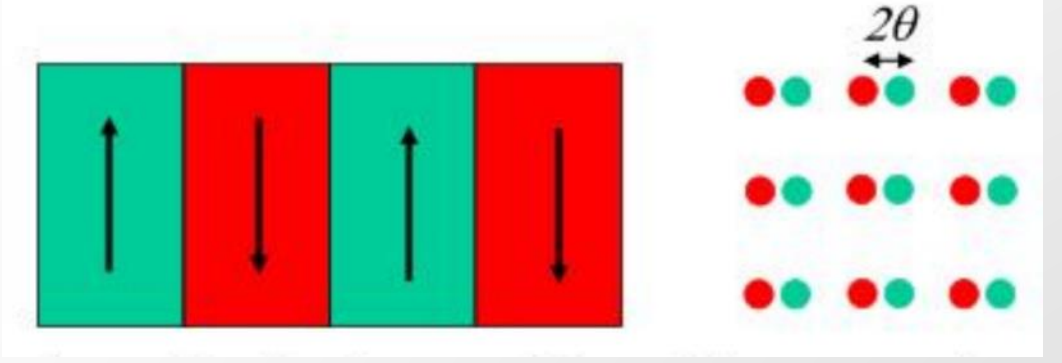
Electrons Objective lens **Aperture** ntensity **Position**

Remember the angle at which electrons are deflected by a magnetic field or potential is more than the order of magnitude smaller than the Bragg angles

$$\theta_L = \frac{\lambda e B_{\perp} t}{h} \approx 50 \mu \text{rad for } \sim 500 \text{mT and } 200 \text{kV electrons}$$

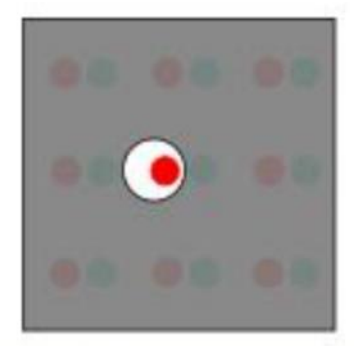
Experimental setup for Foucault Imaging

Take the example of a magnetic sample having domains of opposing \overrightarrow{B} vectors; the diffraction pattern contains slip spots separated by $2\theta_L$

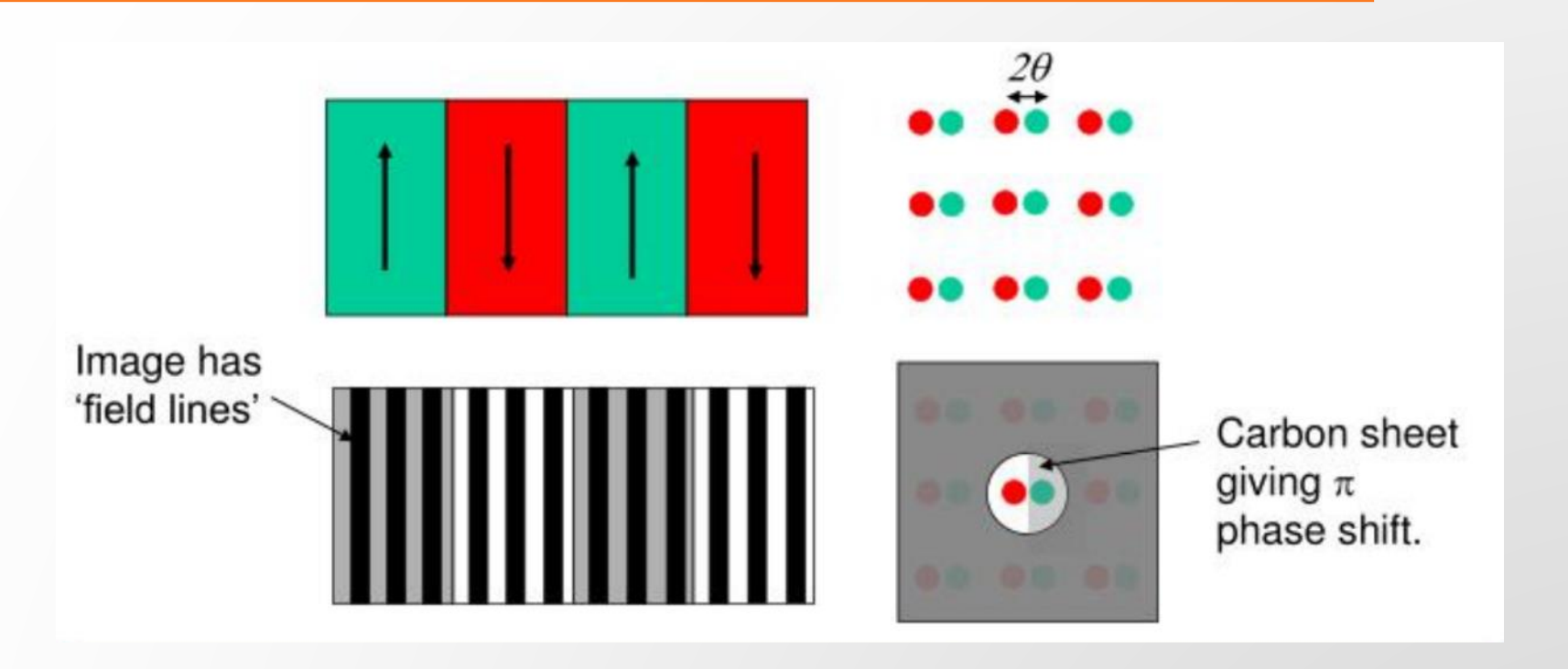


A Foucault image is generated by selecting one of the split spots and using those electrons to form the image intensity (contrast). The dark field or Foucault image exhibits bright intensity having a magnetic induction that allows electrons to pass through the aperture.



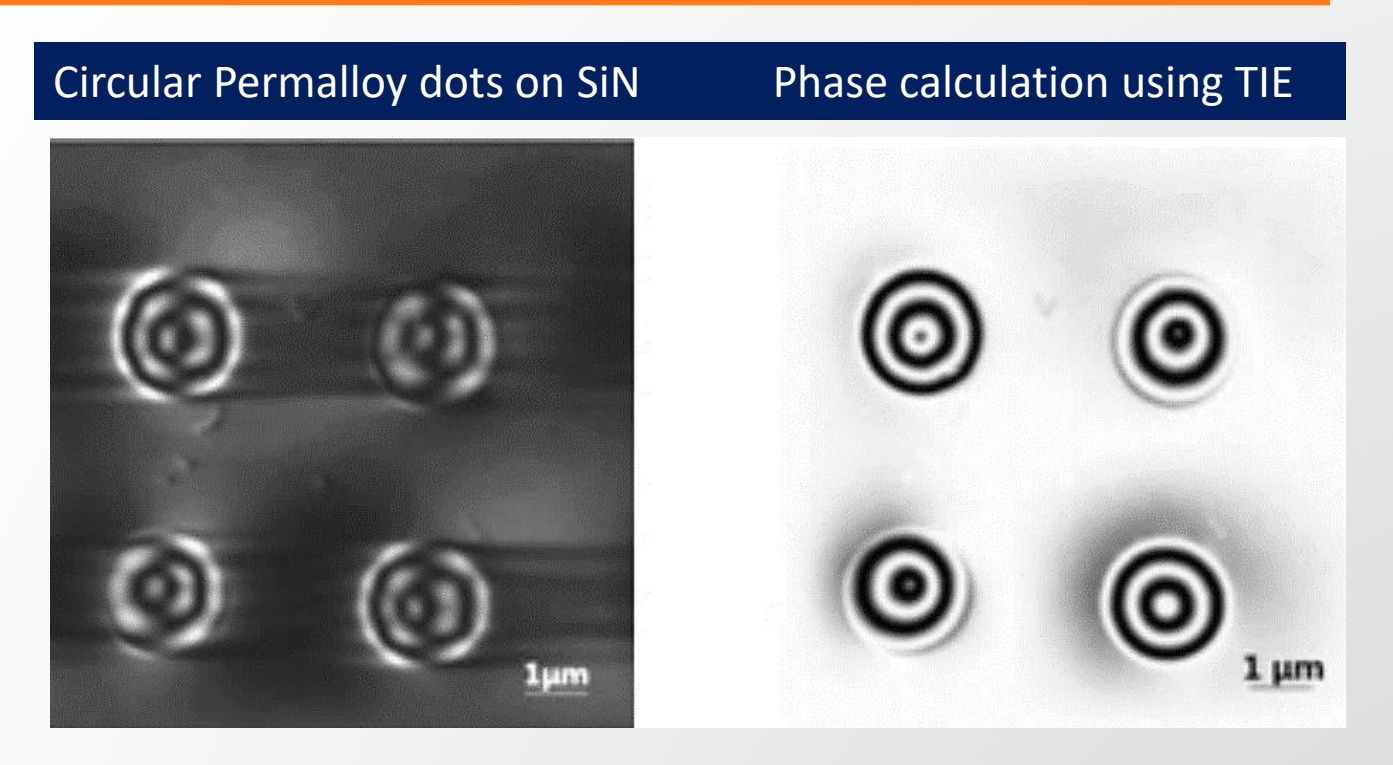


Combining a carbon film phase-plate with Foucault imaging



Instead of selecting one of the split spots to generate a Foucault image, both diffracted spots pass through an aperture partially covered by a carbon film. The thickness of the carbon film is designed to give a π phase shift of the electron beam at a given accelerating voltage, and only one of the spots passes through the film. Under this setup, the Foucault image will contain *Field Lines* within the domains with a 2π phase shift between them.

Combining a carbon film phase-plate with Foucault imaging

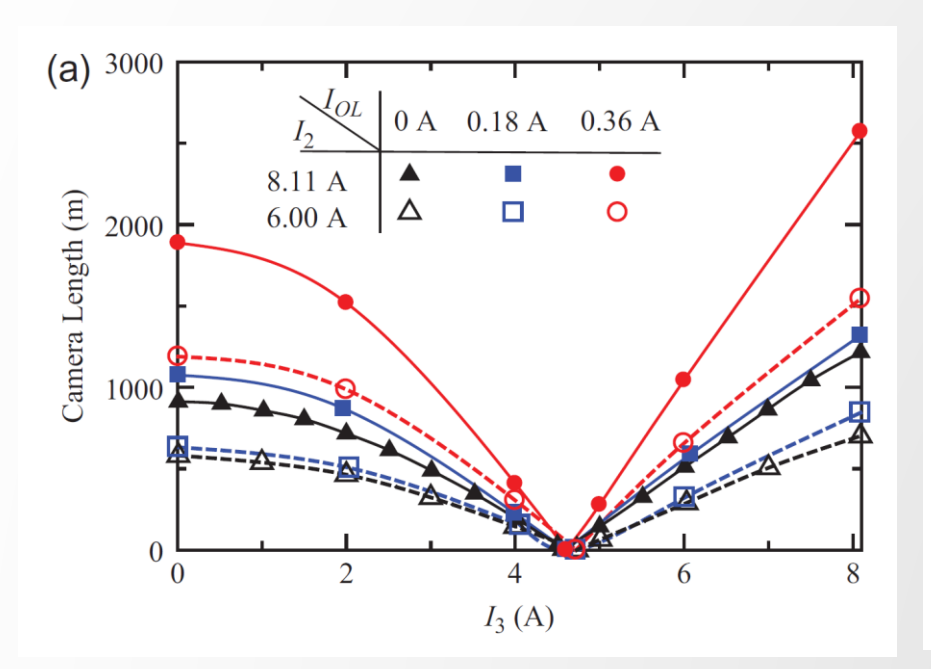


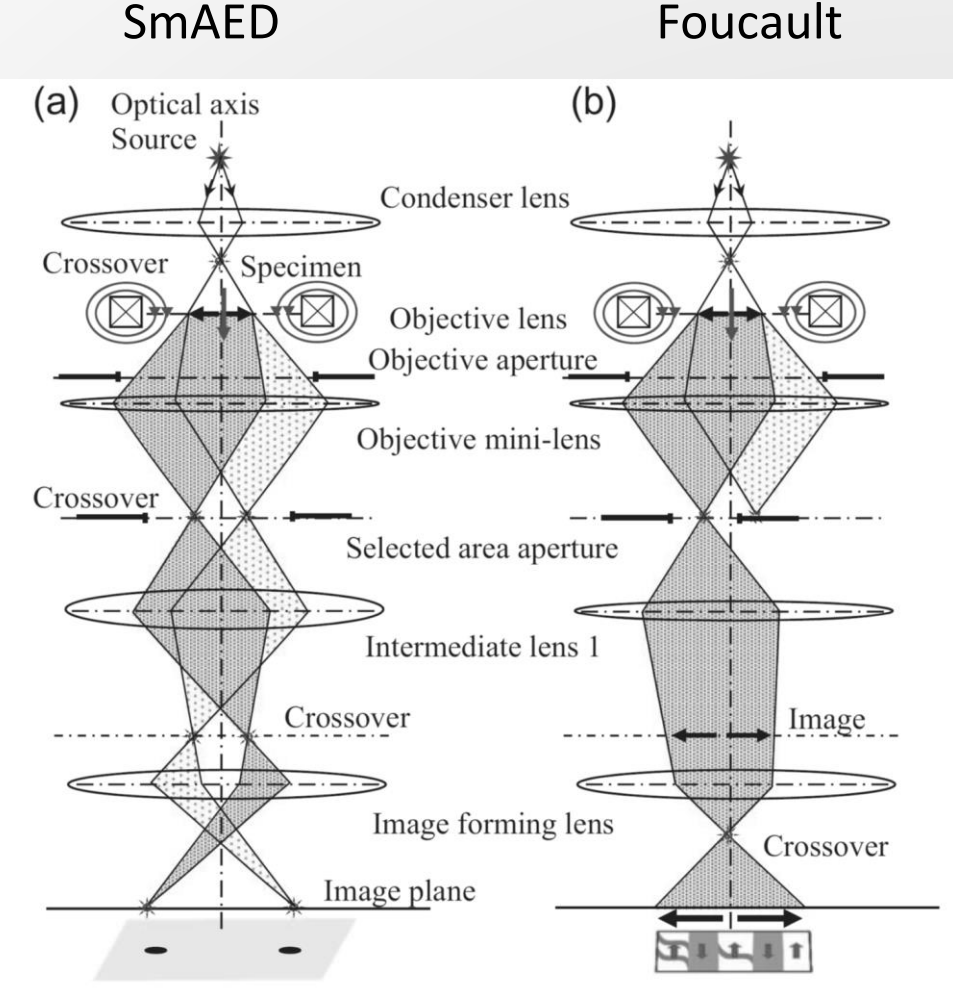
Instead of selecting one of the split spots to generate a Foucault image, both diffracted spots pass through an aperture partially covered by a carbon film. The thickness of the carbon film is designed to give a π phase shift of the electron beam at a given accelerating voltage, and only one of the spots passes through the film. Under this setup, the Foucault image will contain *Field Lines* within the domains with a 2π phase shift between them.

Small Angle Electron Diffraction (SmAED)

SmAED for LTEM studies typically requires camera lengths of 50-1000m

$$\theta_L = \frac{\lambda e B_{\perp} t}{h} \sim 1 - 100 \mu \text{rad}$$



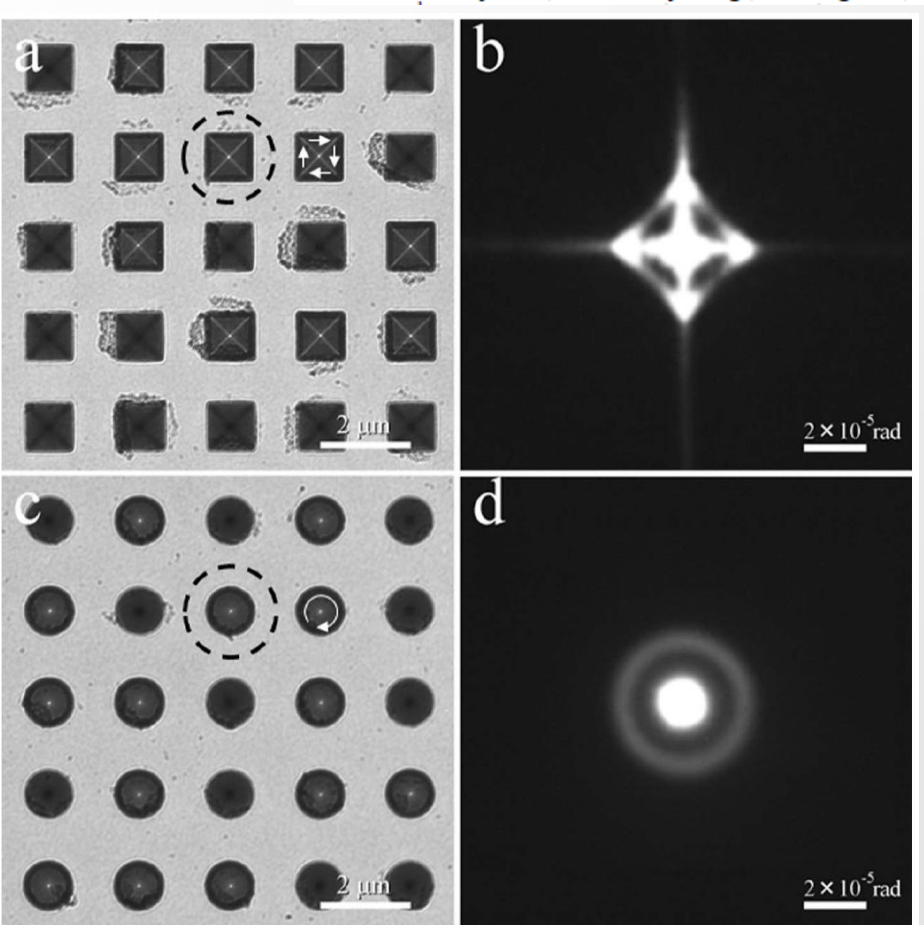


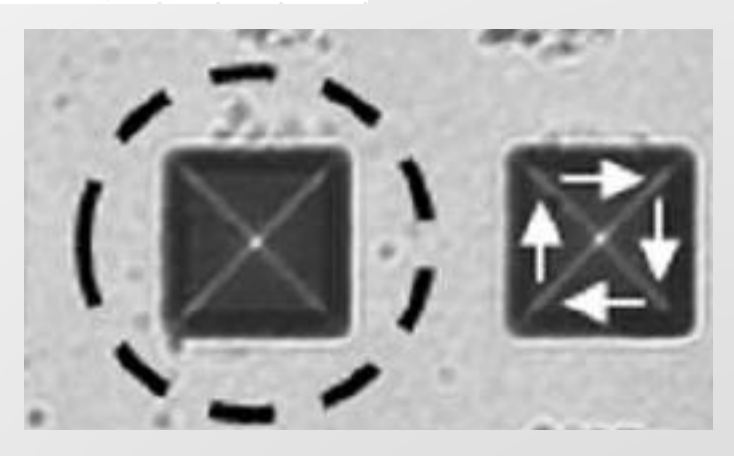
Small Angle Electron Diffraction (SmAED) examples

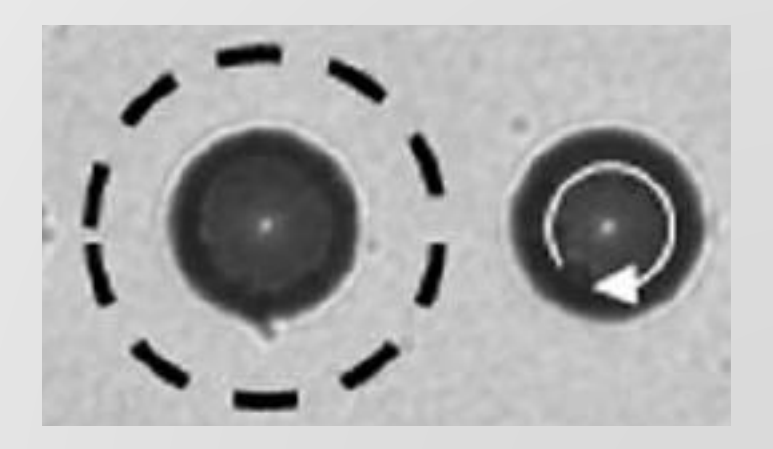
AIP ADVANCES 2, 012195 (2012)

Small angle electron diffraction and deflection

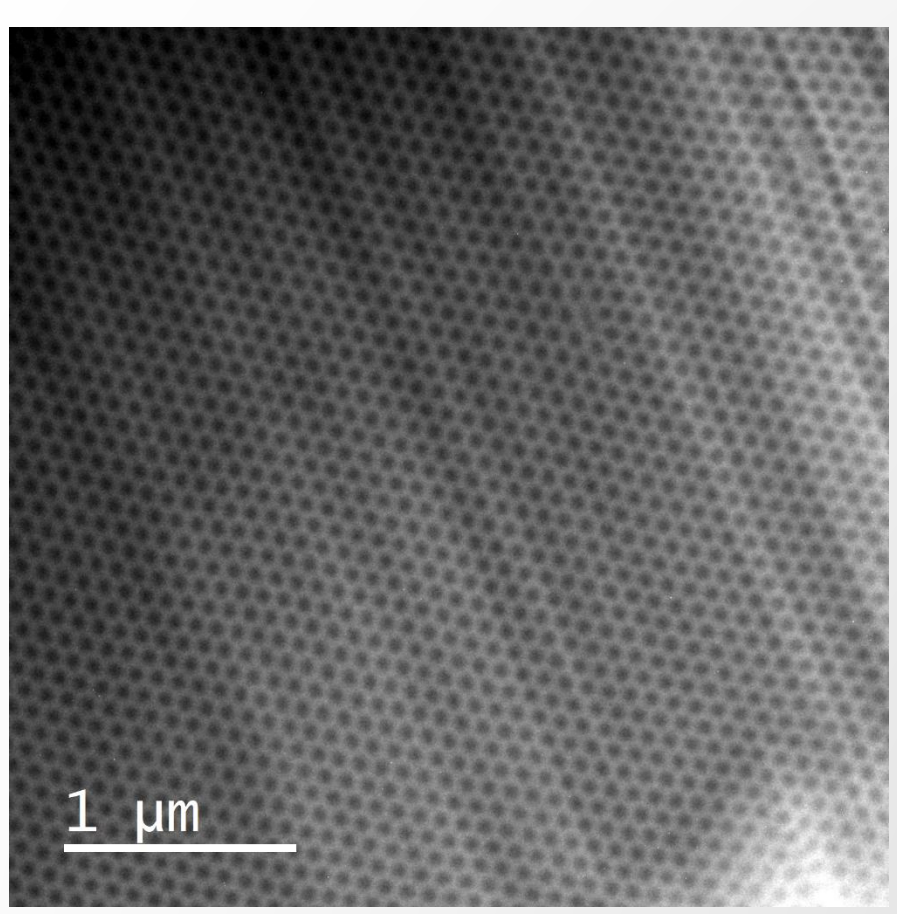
T. Koyama, 1 K. Takayanagi, 2 Y. Togawa, 2,3,a S. Mori, 1,3 and K. Harada 1,4



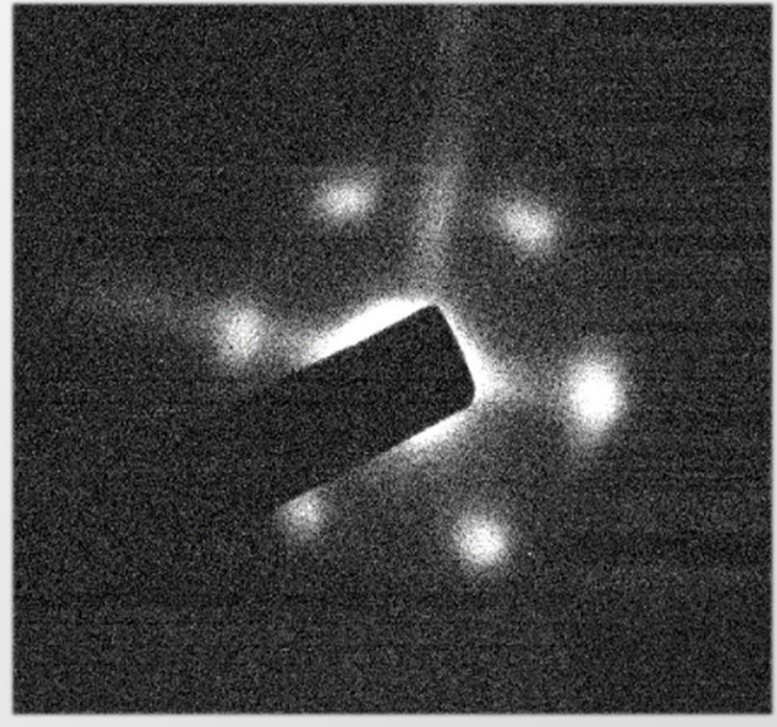




Example: Skyrmion lattice



Small angle electron diffraction of Skyrmion Lattice (SKL)



QUESTIONS?

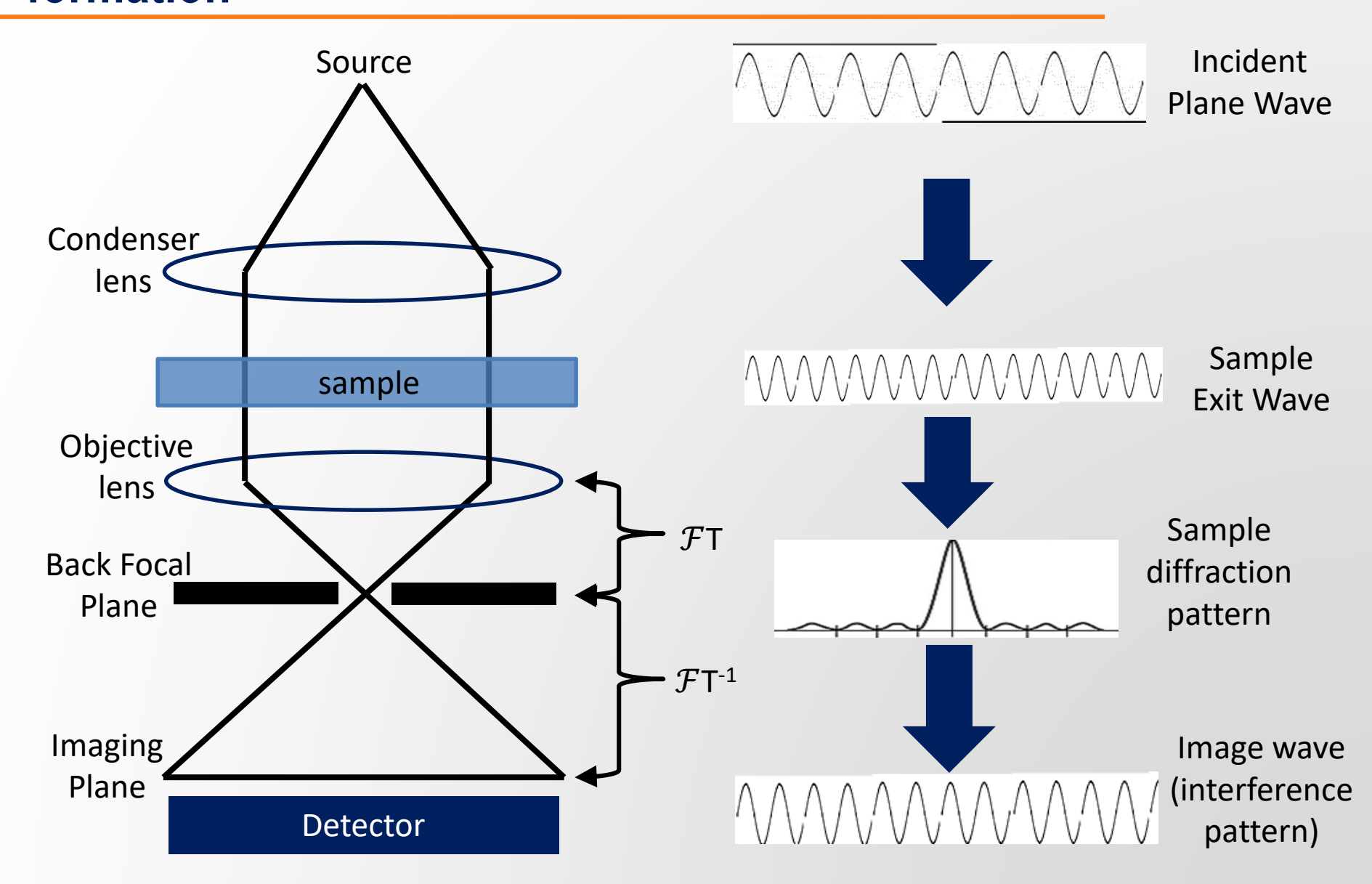


Outline:

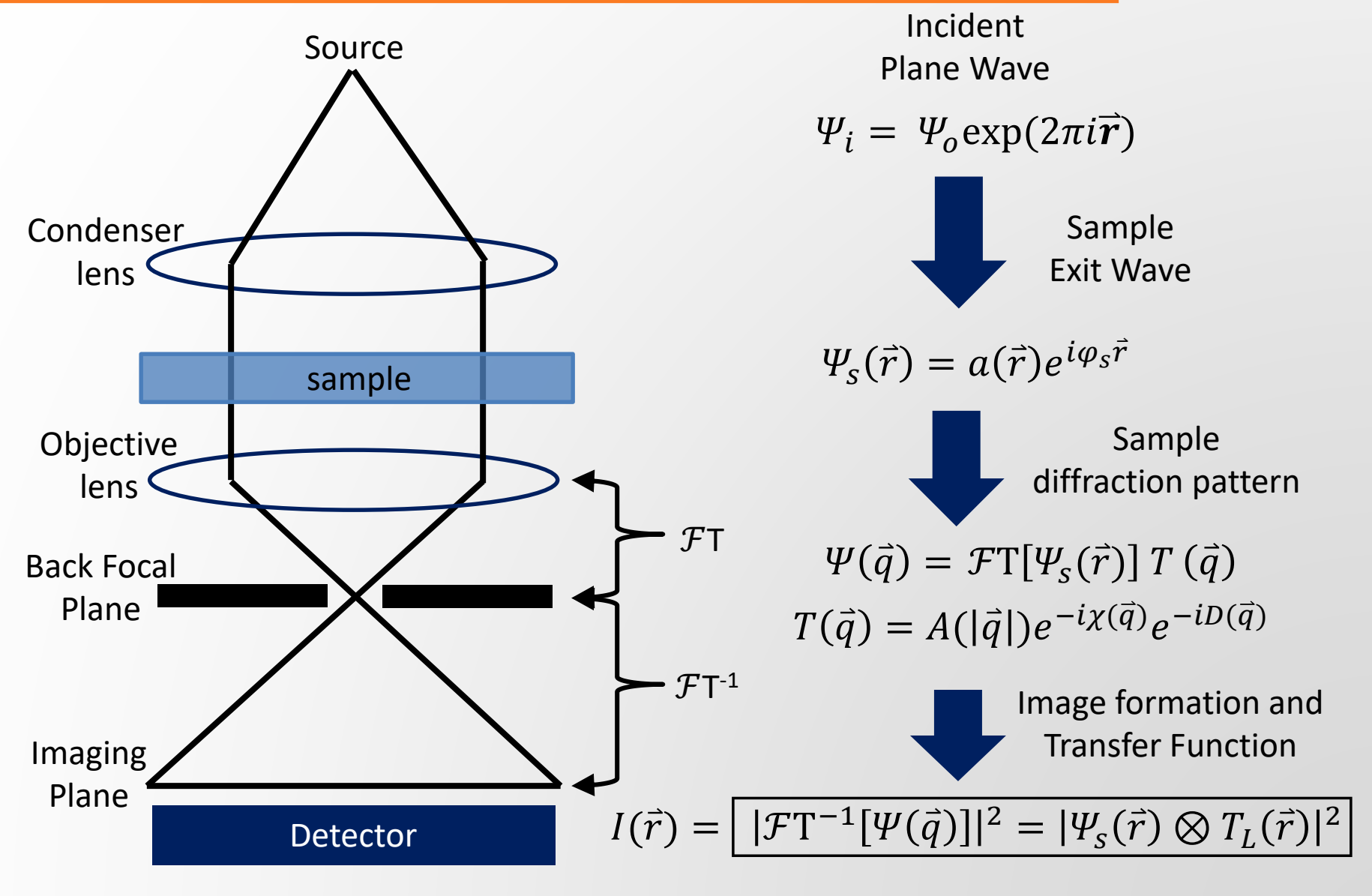
Lorentz microscopy has been used extensively for the past 40 years to study magnetic domain structure and magnetization reversal mechanisms in magnetic thin films and elements. Here, a brief introduction to standard image modes in TEM and the theory involved is presented. The second half of lectures is devoted to discussing how the sample's phase shift and magnetic properties can be quantified from the LTEM observations.

- 1) Lorentz Transmission Electron Microscopy (LTEM)
 - A. Lorentz Force and LTEM Imaging modes
 - B. Fresnel Mode
 - C. Foucault Mode
 - D. Examples
- 2) Simulations and quantitative analysis
 - A. Modeling magnetic images in a real microscope
 - B. Transport of Intensity Equations (TIE)
 - C. Examples

Lorentz image simulation: modeling the TEM image formation



Lorentz image simulation: modeling the TEM image formation



Lorentz image simulation: Transfer function

$$\Psi_{\scriptscriptstyle S}(\vec{r}) = a(\vec{r})e^{i\varphi_{\scriptscriptstyle S}\vec{r}}$$



$$\Psi(\vec{q}) = \mathcal{F}T[\Psi_{S}(\vec{r})] T(\vec{q})$$

$$T_L(\vec{q}) = A[|\vec{q}|]e^{-i\chi(\vec{q})}e^{-iD(\vec{q})}$$



$$\chi(\vec{q}) = \pi \lambda \Delta f \, |\vec{q}|^2 + 1/2\pi C_s \lambda^3 |\vec{q}|^4$$

$$D(\vec{q}) \approx \frac{(\pi \theta_D \Delta f)^2}{\ln 2} |\vec{q}|^2$$

$$T_L(\vec{q}) = A[|\vec{q}|]e^{-i\pi\lambda\Delta f|\vec{q}|^2}e^{-\frac{i(\pi\theta_D\Delta f)^2}{\ln 2}|\vec{q}|^2}$$

The exit wave of the sample, which has the phase shifts associated with both the sample's electrostatic and magnetic potentials

Abbe's equation can be used to approximate imaging (Fourier transform) that is convolved with the microscope transfer function.

 $A[|\vec{q}|]$ is the aperture function (1 inside and 0 outside). Radius and position are varied for Foucault images simulations

 $\chi(\vec{q})$ is the phase function corresponding to the defocus and spherical aberration of the objective lens.

 $D(\vec{q})$ is the damping envelope of the wave function due to the beam divergence and the finite stability of the lenses and accelerator electronics.

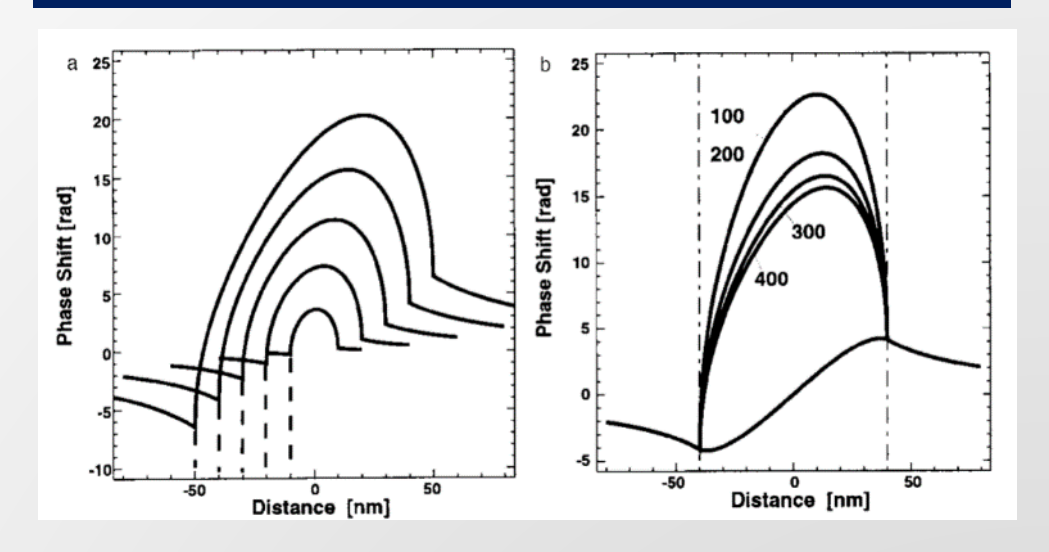
Example: modeling the LTEM Fresnel mode contrast developed by embedded magnetic particles of differing sizes

$\Delta \varphi_m = \frac{-2\pi e}{h} \oint_l \vec{A} dl = \frac{-2\pi e}{h} \int_S \vec{B} dS$ $\Delta \varphi_{m,x} = \frac{2\pi e t}{h} B_y \Delta x$ $\Delta \varphi_{m,y} = \frac{2\pi e t}{h} B_x \Delta y$

Example: J. Dooley and M. De Graef, Micron 28, (1997) p.371

as a function of np size

as a function of HT



For spherical magnetic particles with radius (a),
$$\vec{A}(r) = \frac{4\pi a^3}{3(r^3 > a^3)} M_o[y(\hat{x}\sin\theta + \hat{z}\cos\theta) - z\hat{y}]$$

Assuming that normalized coordinates (e.g.,
$$\bar{r}=\frac{r}{a}$$
, $\bar{y}=\frac{y}{a}$), using $M_o=\frac{3}{8\pi B}$, and $\beta(r,q)=[1-(r^2>1)]^q$

Magnetic phase shift =
$$\frac{\overline{\varphi_m} (r_\perp)}{B_\perp a^2} = \left[\frac{2\pi e \bar{y}}{h\bar{r}^2} \left\{ 1 - \beta \left(\bar{r}, \frac{3}{2} \right) \right\} \right]$$

Electrostatic phase shift =
$$\frac{\overline{\varphi_e(r_\perp)}}{\sigma_E e U_i a} = \boxed{2\left\{\frac{V_m}{V_i} \, \overline{t} - \beta\left(\overline{r}, \frac{1}{2}\right)\right\}}$$

Example: modeling the LTEM Fresnel mode contrast developed by embedded magnetic particles of differing sizes

For embedded magnetic nanoparticles that are strong phase objects, the exit wave follows,

$$\Psi_{S}(\vec{r}) = a(\vec{r})e^{i\left[B_{\perp}a^{2}\overline{\varphi_{m}}(r_{\perp}) + \sigma_{E}eU_{i}a\overline{\varphi_{e}}(r_{\perp})\right]}$$

Imaging of sample information by the microscope lens system can be modeled as,

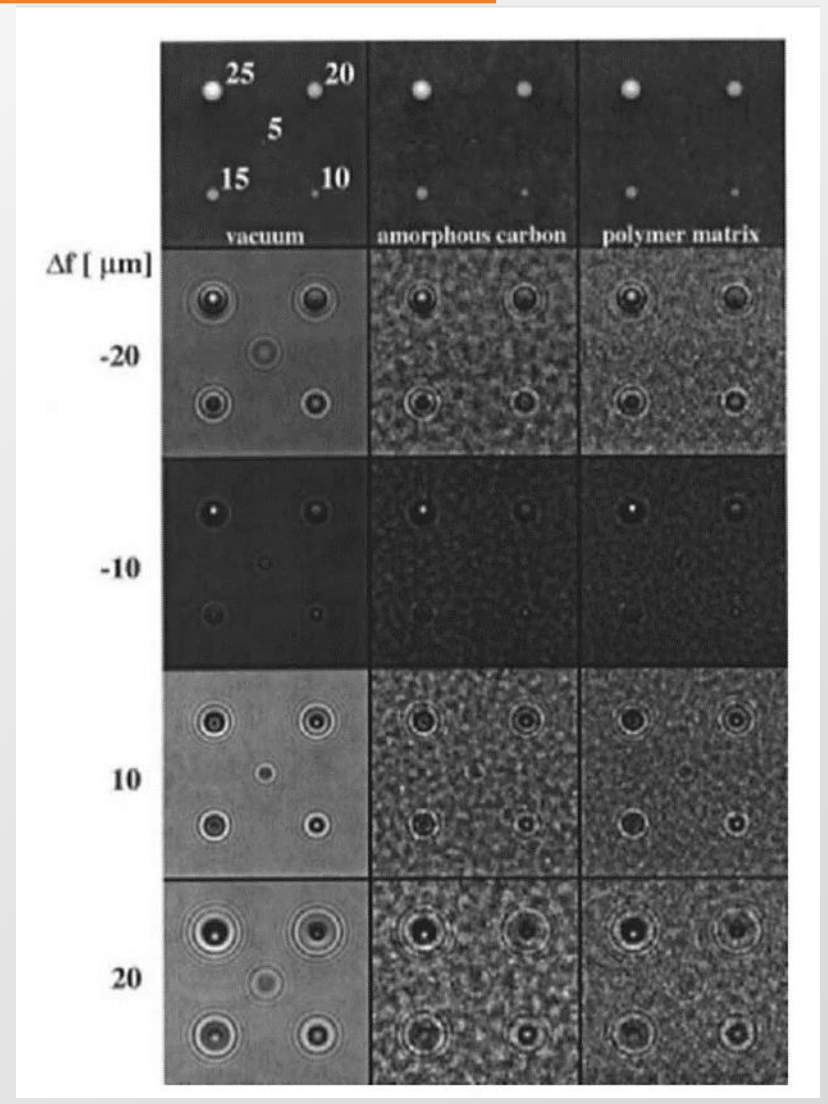
$$\Psi(\vec{q}) = \mathcal{F}T[\Psi_{S}(\vec{r})] T(\vec{q})$$

The transfer function associated with LTEM mode can modeled as,

$$T_L(\vec{q}) = A[|\vec{q}|]e^{-i\pi\lambda\Delta f}|\vec{q}|^2 e^{-\frac{(\pi\theta_D\Delta f)^2}{\ln 2}|\vec{q}|^2}$$

The intensity on the detector plane is the convolution of sample exit wave function and the microscope transfer function

$$I(\vec{r}) = \boxed{|\mathcal{F}\mathbf{T}^{-1}[\Psi(\vec{q})]|^2 = |\Psi_{S}(\vec{r}) \otimes T_{L}(\vec{r})|^2}$$



De Graef, M. (1999). Lorentz microscopy and electron holography of nanocrystalline magnetic materials. <u>Advanced Hard and Soft Magnetic Materials</u>. <u>M. Coey, L. H. Lewis, B. M. Ma et al. Warrendale, Materials Research Society</u>. **577:** 519-530.

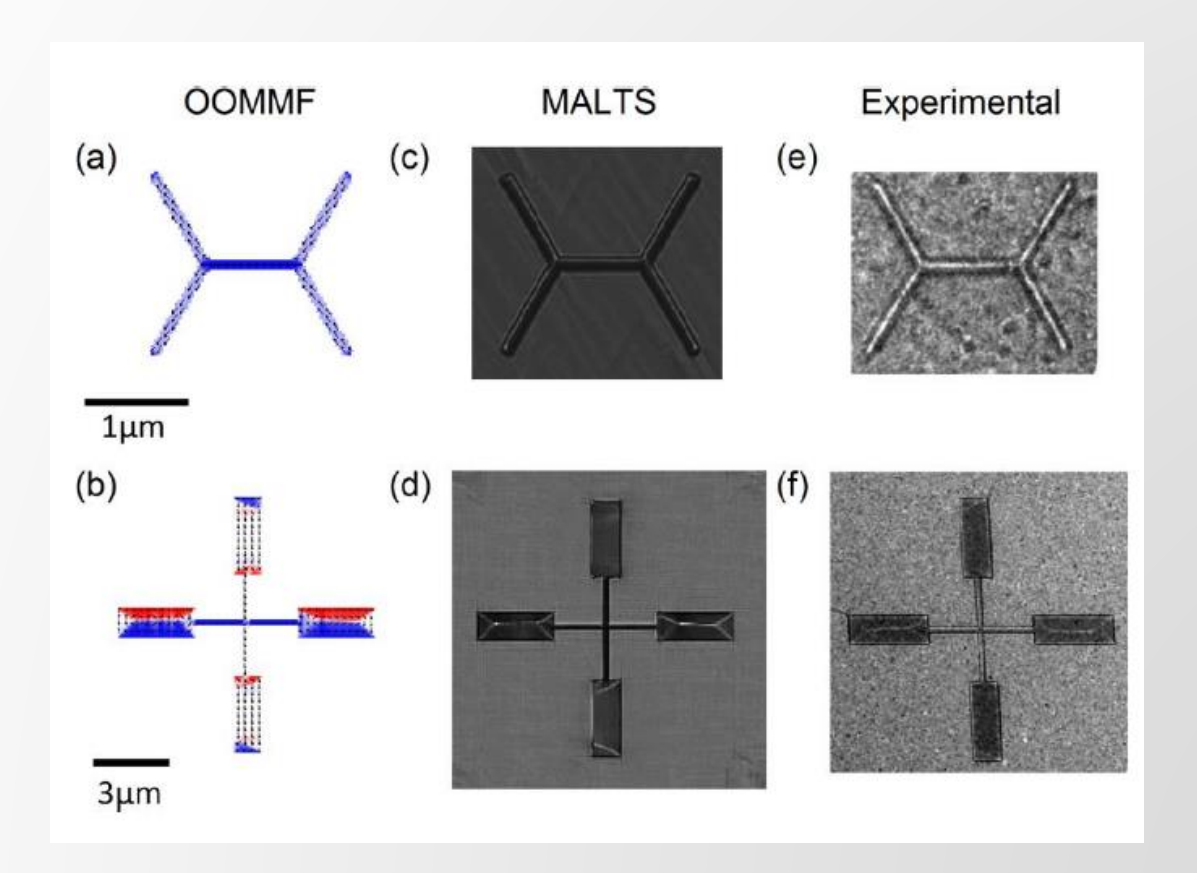
MALTS: Micromagnetic Analysis to Lorentz TEM Simulation

IEEE TRANSACTIONS ON MAGNETICS, VOL. 49, NO. 8, AUGUST 2013

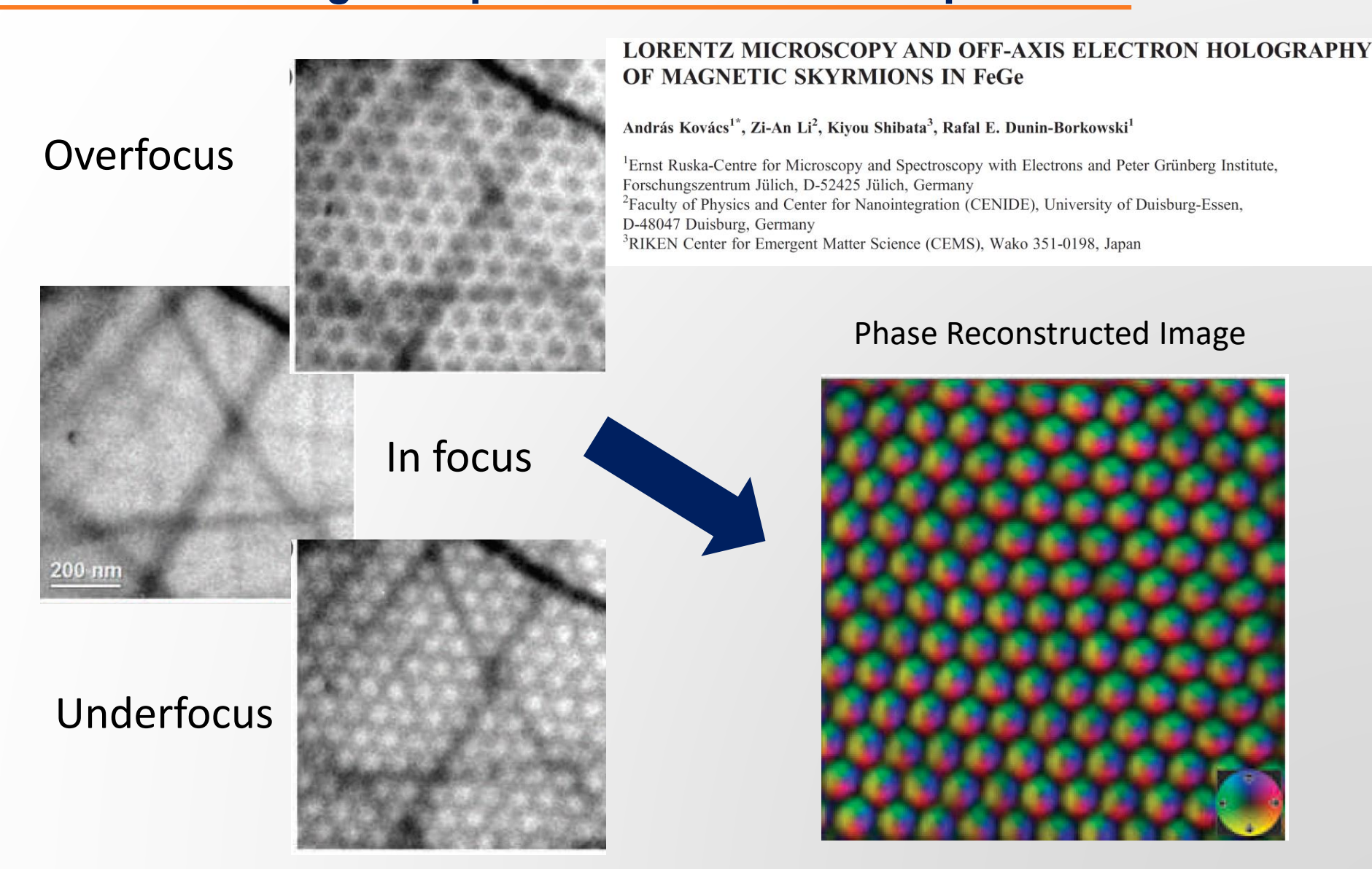
4795

MALTS: A Tool to Simulate Lorentz Transmission Electron Microscopy From Micromagnetic Simulations

Stephanie K. Walton¹, Katharina Zeissler¹, Will R. Branford^{1,2}, and Solveig Felton^{2,3}



How do we model LTEM contrast and be more quantitative about the magnetic phase shifts due to in-plane B



Transport of Intensity Equations (TIE)

For LTEM mode with small deflection angles (i.e., $|\vec{q}_{\perp}|$) and small defocus (Δf) , the phase function $(\chi(\vec{q}))$ and damping envelope $(D(\vec{q}))$ can be written in terms of z and Taylor series expansion of the transfer function (truncating at the quadratic term)

$$\Psi_q(\overrightarrow{q_\perp}) = \mathcal{F}T[\Psi(\overrightarrow{r_\perp})](1 - z|\overrightarrow{q_\perp}|^2)$$

$$z = iz_i + z_r, \quad z_i = \pi\lambda\Delta f \text{ and } z_r = \frac{(\pi\theta_D\Delta f)^2}{\ln 2}$$

The wave function on the image plane (inverse $\mathcal{F}T$) can be written in this general form,

$$\begin{split} \Psi &= ae^{i\varphi} - z\mathcal{F}\mathsf{T}^{-1}\big[\mathcal{F}\mathsf{T}\big(ae^{i\varphi}\big)q^2\big] \quad and \quad \mathcal{F}\mathsf{T}\big(ae^{i\varphi}\big) = f(\overline{q_\perp}) \\ \mathcal{F}\mathsf{T}^{-1}\big[\mathcal{F}\mathsf{T}(ae^{i\varphi})q^2\big] &= \frac{-1}{4\pi^2}\iint f(\overline{q_\perp})\nabla^2 e^{i2\pi\overline{q}_\perp\overline{r_\perp}} \, d\overline{q_\perp} = \frac{-1}{4\pi^2}\nabla^2\big[ae^{i\varphi}\big] \\ \Psi &= ae^{i\varphi} + \frac{z}{4\pi^2}\nabla^2\big[ae^{i\varphi}\big] \end{split}$$

The intensity on the detector plane is the convolution of the sample exit wave function and the microscope transfer function. For uniform illumination ($\nabla^2 a = 0$)

$$I = \left[a^2 - \frac{\lambda \Delta f}{2\pi} \nabla \cdot (a^2 \nabla \varphi) + \frac{(\theta_D \Delta f)^2}{\ln 2} [a \nabla^2 a - a^2 (\nabla \varphi)^2] \right]$$

Transport of Intensity Equations (TIE)

Let's consider 3 cases, infocus (i.e, $I(\vec{r}_{\perp},0)=a^2$), overfocus and underfocus with the same magnitude $|\Delta f|$

Underfocus $I(\vec{r}_{\perp}, -|\Delta f|)$

$$= I(\vec{r}_{\perp}, 0) - \frac{\lambda |\Delta f|}{2\pi} \nabla \cdot (I(\vec{r}_{\perp}, 0) \nabla \varphi) + \frac{(\theta_D |\Delta f|)^2}{\ln 2} \left[\sqrt{I(\vec{r}_{\perp}, 0)} \nabla^2 \sqrt{I(\vec{r}_{\perp}, 0)} - I(\vec{r}_{\perp}, 0) (\nabla \varphi)^2 \right]$$

and for overfocus $I(\vec{r}_{\perp}, +|\Delta f|)$

$$= I(\vec{r}_{\perp}, 0) + \frac{\lambda |\Delta f|}{2\pi} \nabla \cdot (I(\vec{r}_{\perp}, 0) \nabla \varphi) + \frac{(\theta_D |\Delta f|)^2}{\ln 2} \left[\sqrt{I(\vec{r}_{\perp}, 0)} \nabla^2 \sqrt{I(\vec{r}_{\perp}, 0)} - I(\vec{r}_{\perp}, 0) (\nabla \varphi)^2 \right]$$

Subtracting the second equation from the first and rearranging the terms,

$$-\frac{2\pi}{\lambda} \frac{\left(I(\vec{r}_{\perp}, |\Delta f|) - I(\vec{r}_{\perp}, -|\Delta f|)\right)}{2|\Delta f|} = \nabla \cdot \left[I(\vec{r}_{\perp}, 0)\nabla\varphi\right]$$

If we take the limit in a vanishingly small defocus, we arrive at the so-called generalized form of the Transport of Intensity Equation (TIE)

$$\nabla \cdot [I(\vec{r}_{\perp}, 0)\nabla \varphi] = \nabla^2 \Psi = \boxed{-\frac{2\pi}{\lambda} \frac{\partial I(\vec{r}_{\perp}, 0)}{\partial z}}$$

Simplification of the TIE equation

The Transport of Intensity Equation (TIE)

$$\nabla(I(\vec{r}_{\perp},0)\nabla\varphi) = -\frac{2\pi}{\lambda}\frac{\partial I}{\partial z}$$

If the in-focus intensity is constant (I_o) associated with the sample, then,

$$I_o \nabla^2 \varphi = -\frac{2\pi}{\lambda} \frac{\partial I}{\partial z}$$

Implementing a 2-D Fourier transform of the images,

$$-4\pi^2 q^2 \varphi = -\frac{2\pi}{\lambda I_o} \mathcal{F} T \left[\frac{\partial I}{\partial z} \right]$$

rewriting the equation

$$\varphi \approx \frac{1}{2\pi q^2 \lambda I_o} \mathcal{F} T \left[\frac{I(\Delta f) - I(-\Delta f)}{2\Delta f} \right]$$

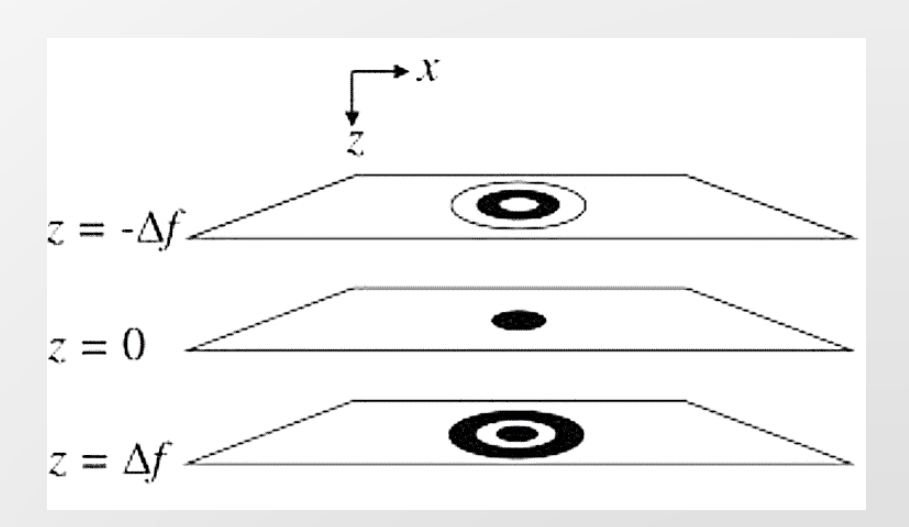
Experimental approach for calculating the phase

$$\varphi \approx \frac{1}{2\pi q^2 \lambda I_o} \mathcal{F} T \left[\frac{I(\Delta f) - I(-\Delta f)}{2\Delta f} \right]$$

$$\nabla \Psi = I(\vec{r}_{\perp}, 0) \nabla \varphi$$

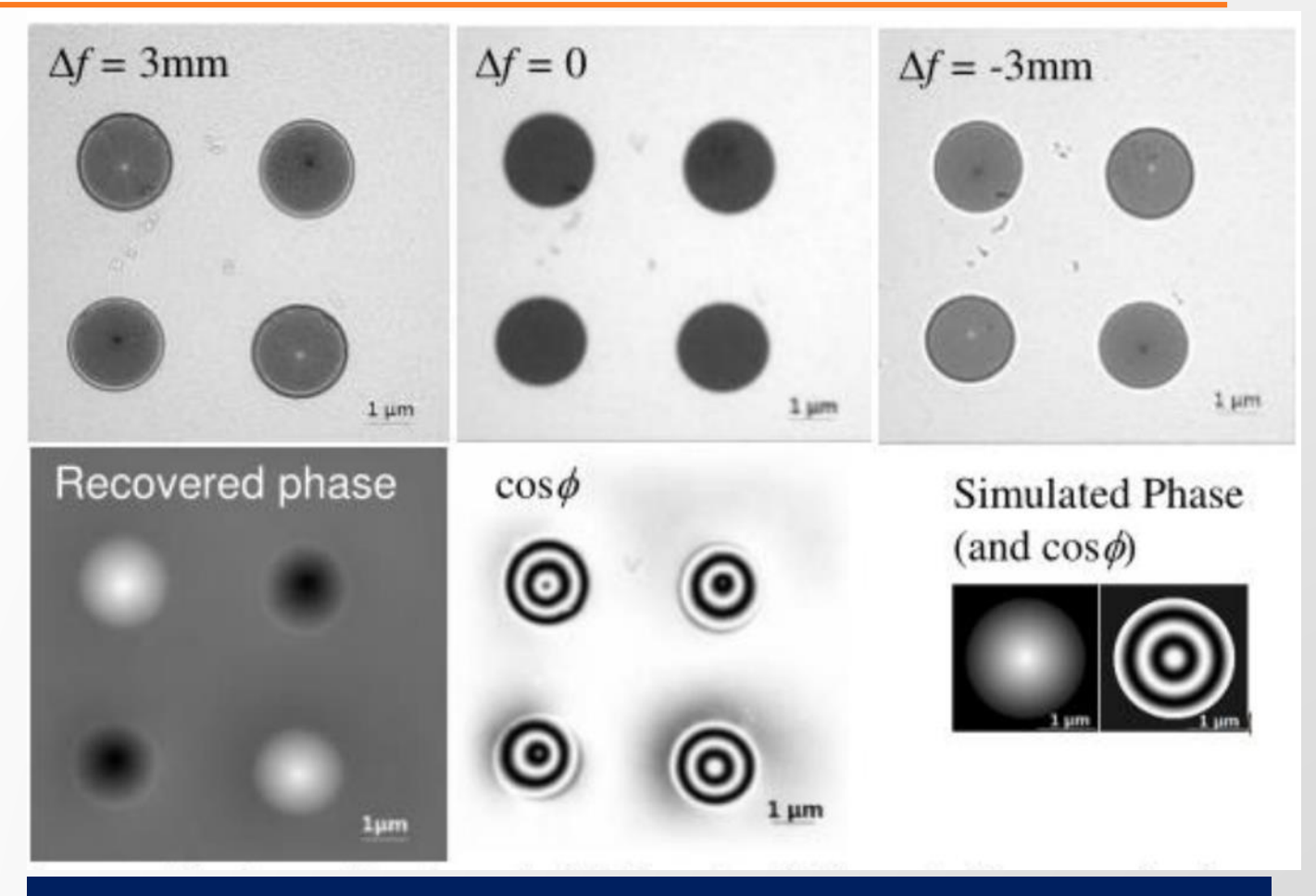
$$\nabla \cdot \nabla \Psi = \nabla^2 \Psi = -\frac{2\pi}{\lambda} \frac{\partial I}{\partial z}$$

$$\nabla \varphi = \frac{\nabla \Psi}{I(\vec{r}_{\perp}, 0)} = -\frac{2\pi e}{h} \left[\vec{B}(r_{\perp}) \times \hat{n} \right] t(r_{\perp})$$



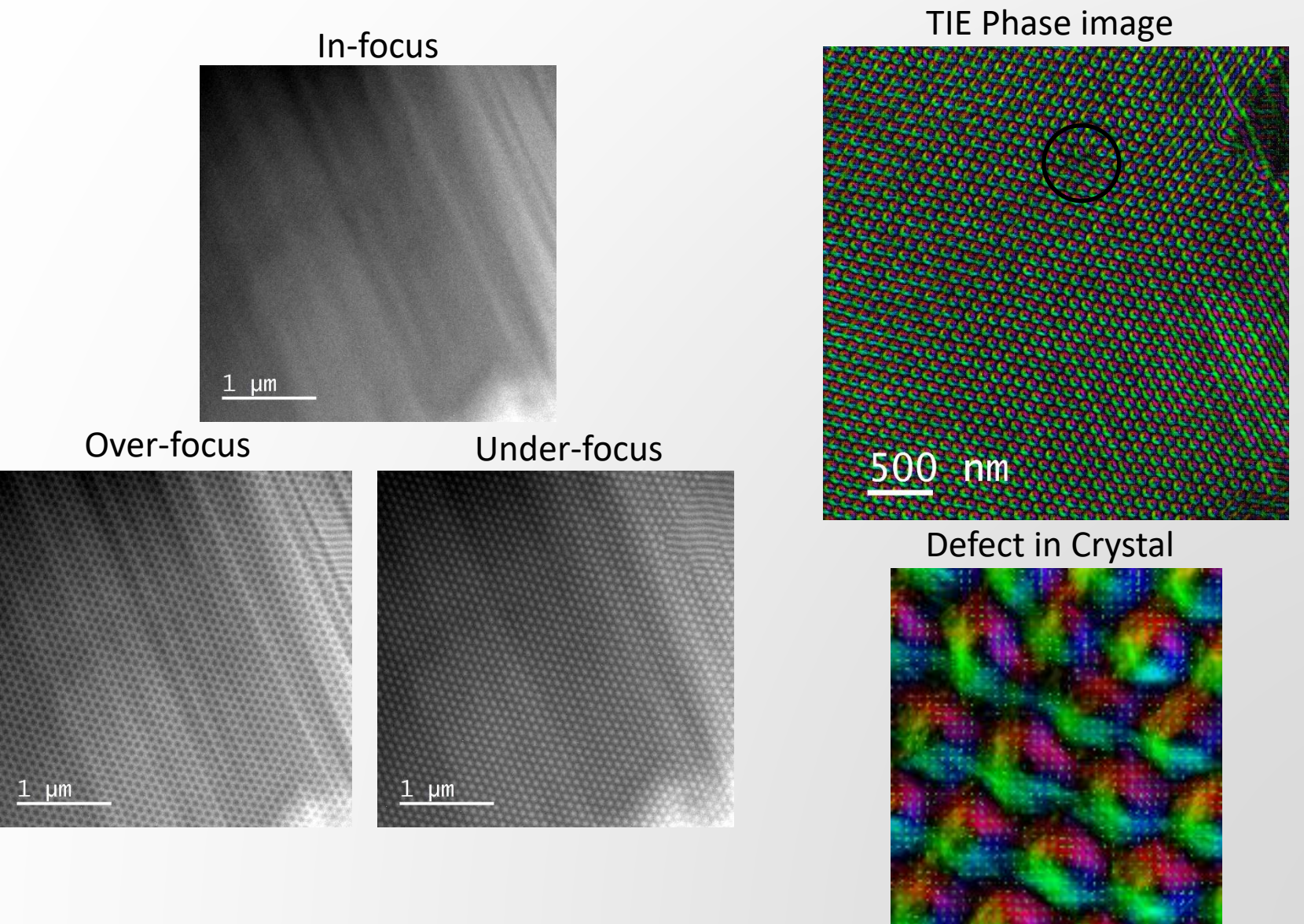
To calculate the phase, images of the same region are taken at overfocus (Δf) , in-focus $(\Delta f = 0)$, and underfocus $(-\Delta f)$. Subtract the overfocus and underfocus, take the Fourier transform, and then divide reciprocal q^2 and constants (in-focus image I_o). The phase is obtained by the inverse $\mathcal{F}T^{-1}$ of this quantify.

Example: permalloy disks deposited on SiN membrane

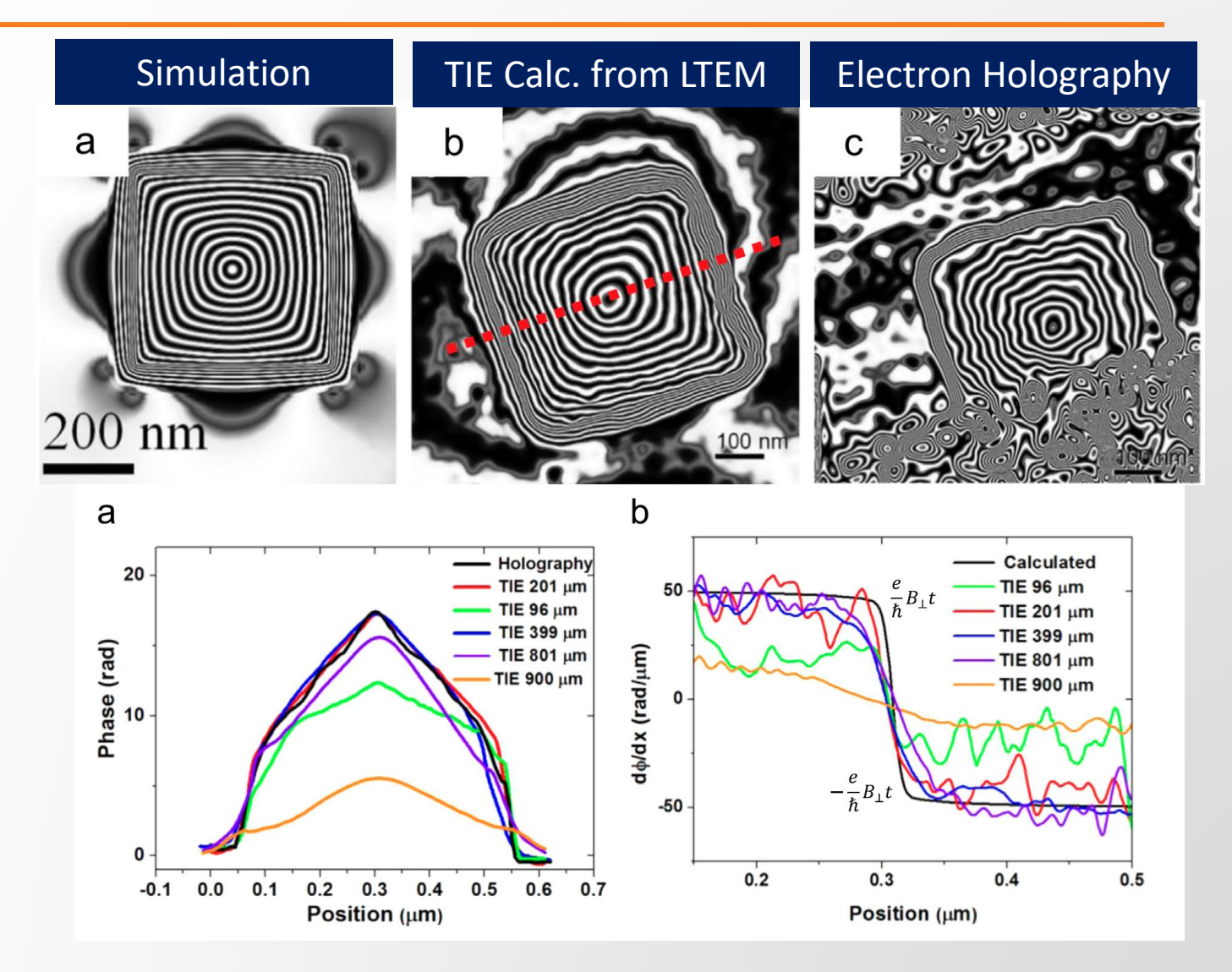


It is convenient to display the calculated phase images as "cosine of the phase" contour map in which there is a phase shift of 2π between the dark lines that resembles the magnetic field lines.

Example: TIE of Skyrmions in FeGe (unpublished results)



Comparison with electron holography



A. Kohn, A. Habibi, M. Mayo, Ultramicroscopy160(2016)44–56

Resolution, optimal defocus, and accuracy of calculated phase using TIE

Phase Measurement in Electron Microscopy Using the Transport of Intensity Equation

Kazuo Ishizuka, and Brendan Allman*

HREM Research Inc, *IATIA Ltd

$$\frac{(\pi\lambda\Delta f q_{max}^2)}{3!} \le c \ll 1, c \sim 0.25$$

Table 1. Upper limits of defocus for the three-image case

| d _{min} (nm) | πλ(2Δf) | 100 kV | 200 kV | 400 kV |
|-----------------------|------------------------|---------|---------|---------|
| 0.14 | 4.90 x10 ⁻² | 4.2 nm | 6.2 nm | 9.5 nm |
| 0.2 | 9.80x 10 ⁻² | 8.4 nm | 19.0 nm | 19.0 nm |
| 1 | 2.45 | 211 nm | 311 nm | 474 nm |
| 10 | 2.45 x10 ² | 21.1 µm | 31.1 µm | 47.4 μm |
| 100 | 2.45 x10 ⁴ | 2.11 mm | 3.11 mm | 4.74 mm |

QUESTIONS?



Bibliography

- 1. Budruk, A., et al., *In situ lorentz TEM magnetization study of a Ni–Mn–Ga ferromagnetic shape memory alloy.* Acta Materialia, 2011. **59**(12): p. 4895-4906.
- 2. Chapman, J.N., A.B. Johnston, and L.J. Heyderman, *Coherent Foucault imaging: A method for imaging magnetic domain structures in thin films.* Journal of Applied Physics, 1994. **76**(9): p. 5349-5355.
- 3. De Graef, M., Lorentz microscopy and electron holography of nanocrystalline magnetic materials, in Advanced Hard and Soft Magnetic Materials, M. Coey, et al., Editors. 1999, Materials Research Society: Warrendale. p. 519-530.
- 4. De Graef, M., 2. Lorentz microscopy: Theoretical basis and image simulations, in Experimental Methods in the Physical Sciences, M. De Graef and Y. Zhu, Editors. 2001, Academic Press. p. 27-67.
- 5. De Graef, M. and Y. Zhu, *Magnetic Imaging and Its Applications to Materials*. Experimental methods in the Physic Sciences, ed. R. Celotta and T. Lucatorto. Vol. 36. 2000, London, UK: Elsevier Science.
- 6. Dooley, J. and M. De Graef, Energy filtered magnetic induction mapping. Micron, 1997. 28(5): p. 371-380.
- 7. Gureyev, T.E. and K.A. Nugent, *Phase retrieval with the transport-of-intensity equation .2. Orthogonal series solution for nonuniform illumination.* Journal of the Optical Society of America a-Optics Image Science and Vision, 1996. **13**(8): p. 1670-1682.
- 8. Gureyev, T.E., A. Roberts, and K.A. Nugent, *PHASE RETRIEVAL WITH THE TRANSPORT-OF-INTENSITY EQUATION MATRIX SOLUTION WITH USE OF ZERNIKE POLYNOMIALS.* Journal of the Optical Society of America a-Optics Image Science and Vision, 1995. **12**(9): p. 1932-1941.
- 9. Gureyev, T.E., A. Roberts, and K.A. Nugent, *PARTIALLY COHERENT FIELDS, THE TRANSPORT-OF-INTENSITY EQUATION, AND PHASE UNIQUENESS.* Journal of the Optical Society of America a-Optics Image Science and Vision, 1995. **12**(9): p. 1942-1946.
- 10. Kohn, A., A. Habibi, and M. Mayo, *Experimental evaluation of the 'transport-of-intensity' equation for magnetic phase reconstruction in Lorentz transmission electron microscopy.* Ultramicroscopy, 2016. **160**: p. 44-56.

Bibliography

- 11. Kotani, A., et al., Lorentz microscopy and small-angle electron diffraction study of magnetic textures in La1-xSrxMnO3 (0.15 < x < 0.30): The role of magnetic anisotropy. Physical Review B, 2016. **94**(2): p. 7.
- 12. Koyama, T., et al., Small angle electron diffraction and deflection. AIP Advances, 2012. 2.
- 13. McVitie, S. and M. Cushley, *Quantitative Fresnel Lorentz microscopy and the transport of intensity equation*. Ultramicroscopy, 2006. **106**(4-5): p. 423-431.
- 14. Nakajima, H., et al., *Foucault imaging and small-angle electron diffraction in controlled external magnetic fields.* Microscopy, 2016. **65**(6): p. 473-478.
- 15. Nakajima, H., et al., *Foucault optical system by using a nondedicated conventional TEM.* Surface and Interface Analysis, 2016. **48**(11): p. 1166-1168.
- 16. Paganin, D. and K.A. Nugent, *Noninterferometric phase imaging with partially coherent light.* Physical Review Letters, 1998. **80**(12): p. 2586-2589.
- 17. Phatak, C., A.K. Petford-Long, and M. De Graef, *Recent advances in Lorentz microscopy*. Current Opinion in Solid State and Materials Science, 2016. **20**(2): p. 107-114.
- 18. Portier, X., et al., Lorentz transmission electron microscopy on NiFe/Cu/Co/NiFe/MnNi active spin valve elements. Applied Physics Letters, 1997. **71**(14): p. 2032-2034.
- 19. Taniguchi, Y., H. Matsumoto, and K. Harada, *Foucault imaging by using non-dedicated transmission electron microscope*. Applied Physics Letters, 2012. **101**(9): p. 4.
- 20. Volkov, V.V. and Y. Zhu, Magnetic structure and microstructure of die-upset hard magnets RE13.75Fe80.25B6 (RE = Nd, Pr): A possible origin of high coercivity. Journal of Applied Physics, 1999. **85**(6): p. 3254-3263.
- 21. Zhang, S., et al., *Creation of a thermally assisted skyrmion lattice in Pt/Co/Ta multilayer films*. Applied Physics Letters, 2018. **113**(19): p. 192403.

Practical considerations for doing TIE analysis

Difficulties and Errors with TIE phase retrieval: Noise

To understand noise effects on the phase recovery, consider a wave with no intensity modulation but has a phase distribution

$$k\frac{\partial \rho}{\partial z} = -\nabla^2 \varphi$$

Implementing Fourier theory then gives,

$$\frac{2\pi}{\lambda} \mathcal{F} T \left[\frac{\partial \rho}{\partial z} \right] = |q_{\perp}|^2$$

Where q_{\perp} is the spatial frequency, the solution phase follows,

$$\varphi = \frac{2\pi}{\lambda} \mathcal{F} T^{-1} \left[\frac{1}{|q_{\perp}|^2} \mathcal{F} T \left[\frac{\partial \rho}{\partial z} \right] \right]$$

Thus, the phase recover from input data involves the numerical differentiation of experimental data, noise sensitive operation. However, phase recovery with TIE is relatively insensitive to noise even at levels around 10%

Thus, to reduce noise effects, a larger defocus can be used at the expense of reduced spatial resolution

Difficulties and Errors with TIE phase retrieval: Systematic errors, e.g., magnification, image shifts, image rotation

Image shifts

- Suppose an electron plane wave traveling at an angle, θ , can be described by the phase gradient, $\varphi' = \frac{2\pi}{\lambda} \sin \theta$
- If an image (sample) shifts by Δ causing defocus error of δz , then $\varphi' = \frac{2\pi}{\lambda} \frac{\Delta}{\delta z}$
- The acceptable misalignment depends on the extent of phase excursion (size) required to observe a feature.

Magnification errors

- A difference of 1% in magnification can cause significant errors in the recovered phases.
- In an astigmatic system, the magnification can differ with transverse direction, and defocus error-induced magnification changes result in an additional cylindrical phase across the image

Image rotation

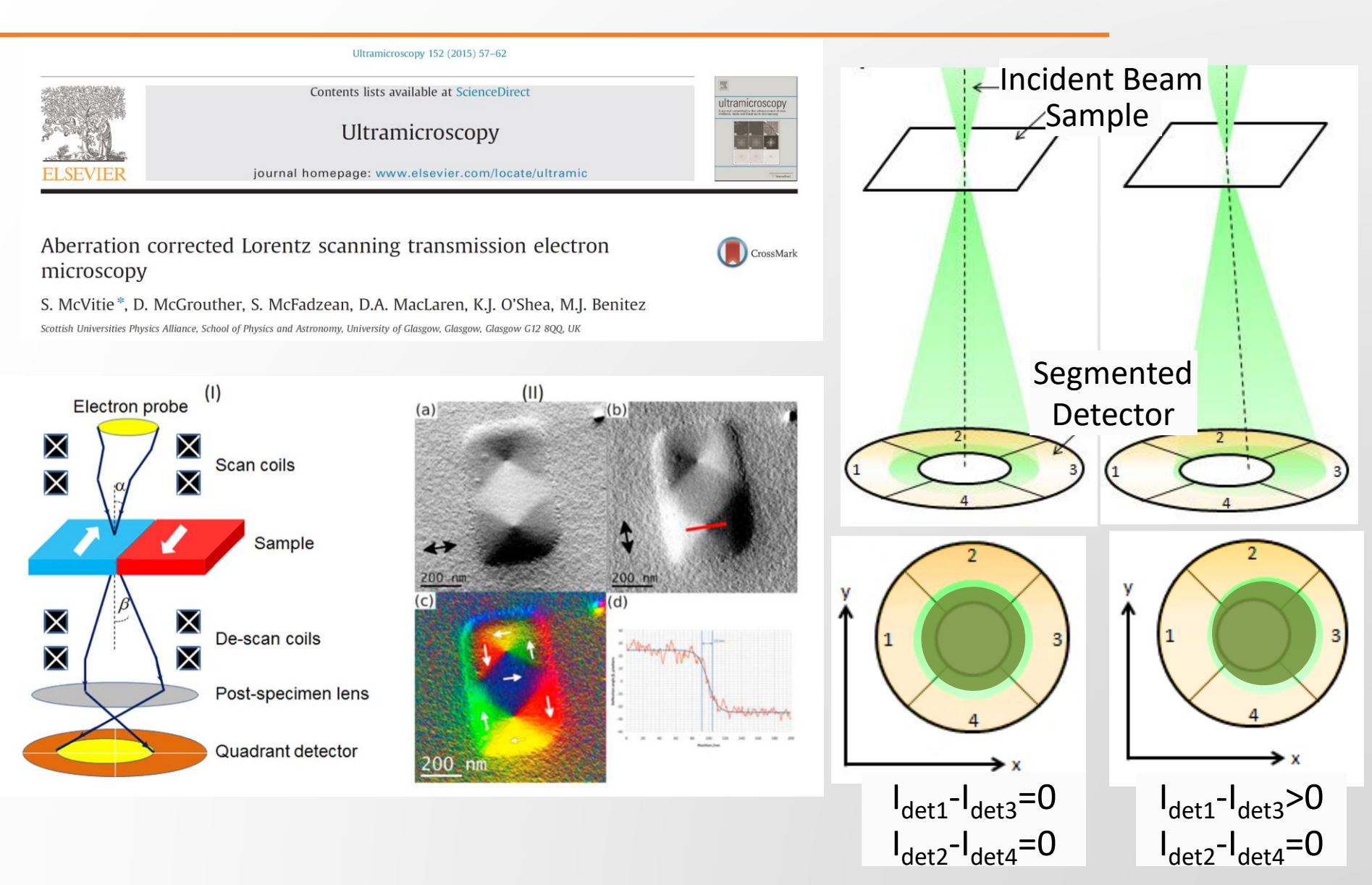
- For phase distribution of $\phi=n\theta$, where θ is the azimuthal angle on intensity distribution, the phase distribution undergoes a differential rotation separated by differential distance.
- A small amount of rotation can create local phase gradients and distortion artifacts.

Image Normalization

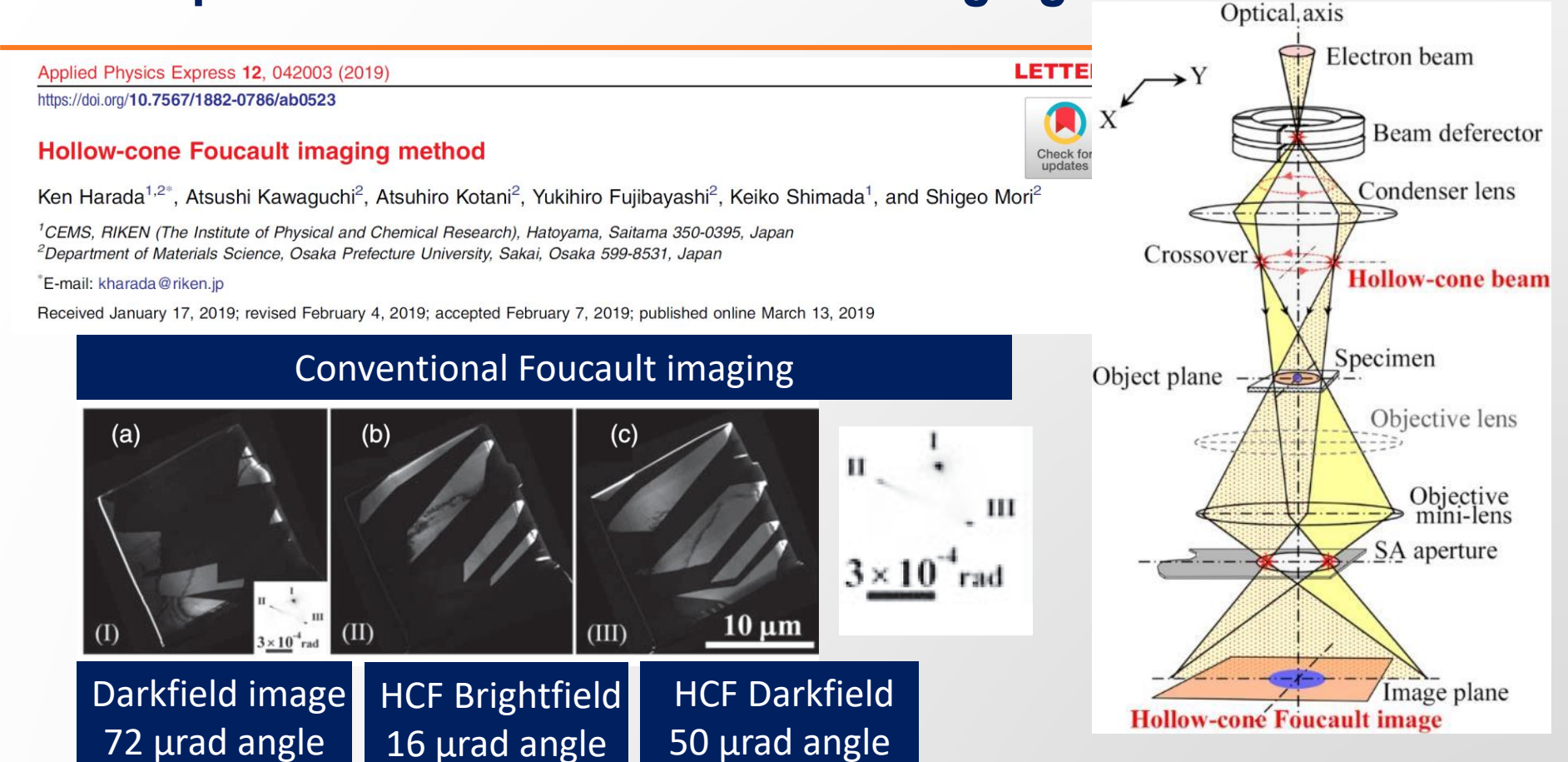
 Incorrect image normalization on the order of <1% can even cause dramatic effects on the recovered phase and image artifacts

Other techniques and examples for imaging magnetic structures in the TEM

Lorentz Scanning TEM and Differential Phase Contrast (DPC)



Examples: Hollow Cone Foucault imaging



Precessing the beam (azimuthal angle) about small tilt angles $(2\theta_L)$ allows imaging all domains and their boundaries with high spatial resolution(~1nm)

thomas.lagrange@epfl.ch • www.epfl.ch • lumes.epfl.ch • +41 (0)21 6935861

(g)

(b)

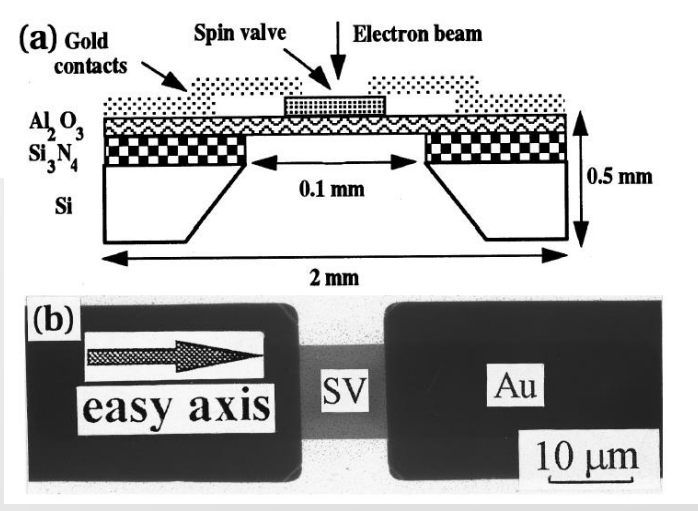
Foucault mode example: in-situ measurements in spintronics

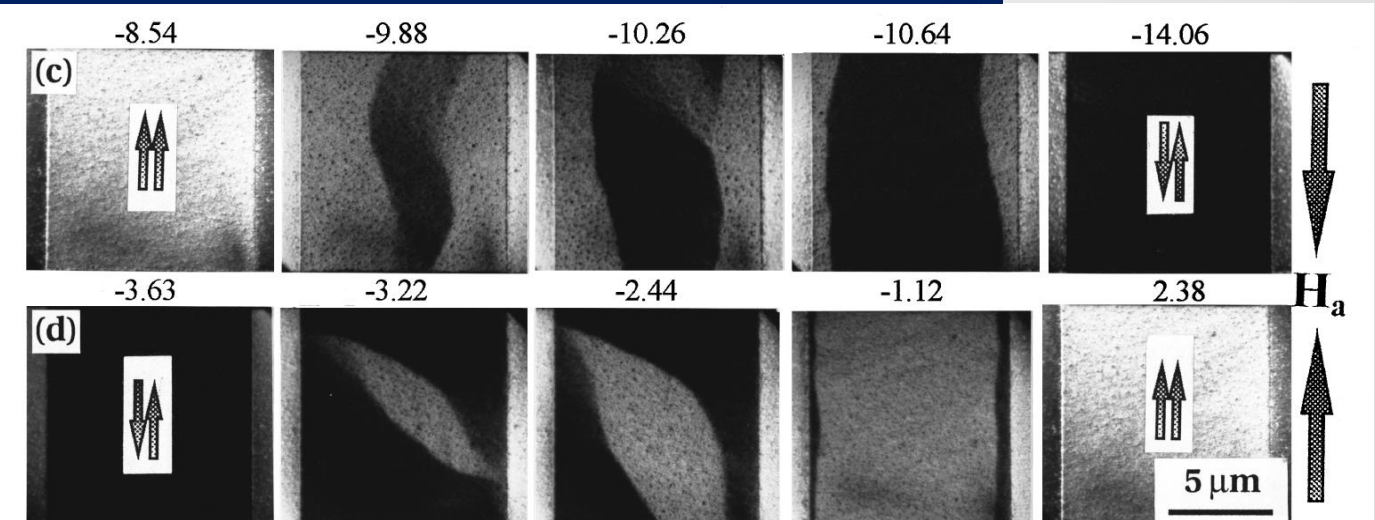
Lorentz transmission electron microscopy on NiFe/Cu/Co/NiFe/MnNi active spin valve elements

X. Portier,^{a)} A. K. Petford-Long, and R. C. Doole Department of Materials, University of Oxford, Oxford OX1 3PH, United Kingdom

T. C. Anthony and J. A. Brug Hewlett-Packard Laboratories, Palo Alto, California, 94304

They observed the magnetic domain structure and made simultaneous magnetoresistance measurements under an applied, controlled field and current in which they correlated changes in the domains to GMR (giant magnotoresitance).

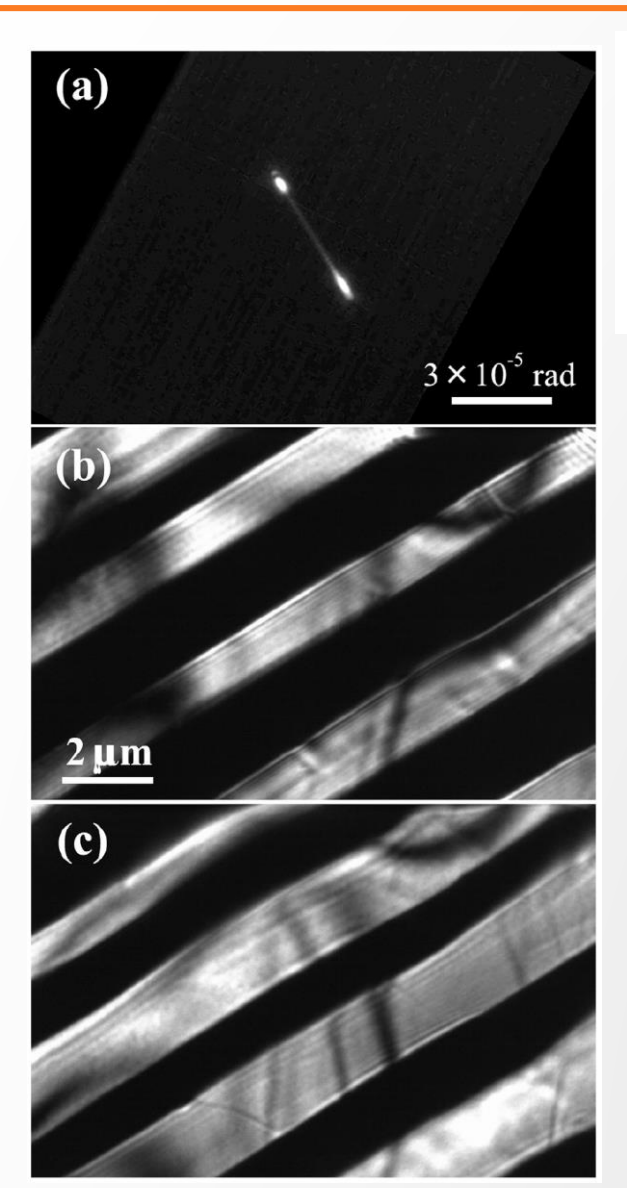




Applied magnetic field in Oersted 1Oe= 0.1 mT

Current density 1.5x10⁶ A cm⁻²

Example: Combining LTEM imaging modes



APPLIED PHYSICS LETTERS 101, 093101 (2012)

Foucault imaging by using non-dedicated transmission electron microscope

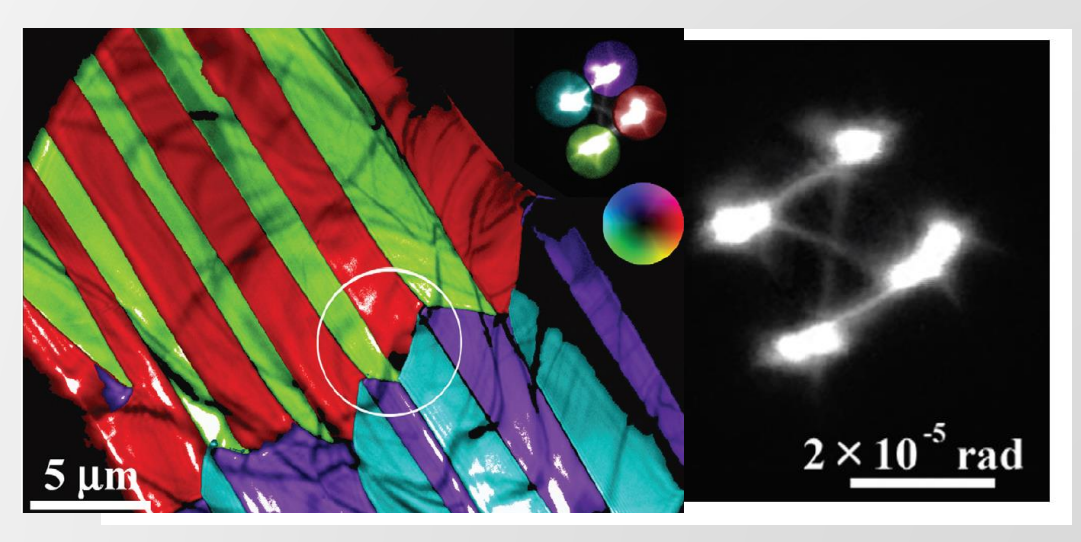
Yoshifumi Taniguchi (谷口佳史), ¹ Hiroaki Matsumoto (松本弘昭), ² and Ken Harada (原田研)^{3,a)}

¹Science and Medical Systems Business Group, Hitachi High-Technologies Corp., Ichige, Hitachinaka, Ibaraki 312-8504, Japan

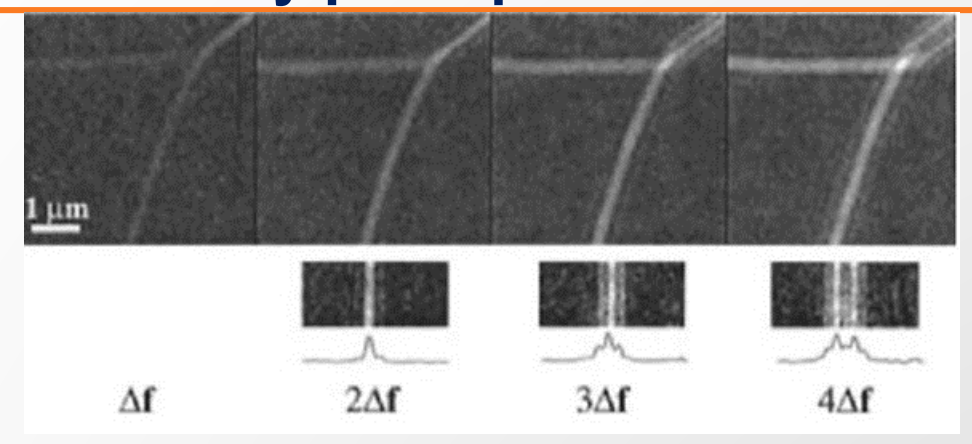
²Corporate Manufacturing Strategy Group, Hitachi High-Technologies Corp., Ishikawa-cho, Hitachinaka, Ibaraki 312-1991, Japan

³Central Research Laboratory, Hitachi Ltd., Hatoyama, Saitama 350-0395, Japan

Combining Small Angle Electron Diffraction (SmAED) with Foucault and Fresnels mode LTEM imaging provides high spatial resolution (1-10nm) and quantification of the magnetic induction vector components.



Quantum mechanical description of Lorentz TEM and Heisenberg uncertainty principle



The classical description of Lorentz deflected beam does not explain the observed fringes in the convergent "bright" domain walls

$$\varphi(y)=rac{2\pi e B_{\perp} {\sf ty}}{h}, \qquad
abla arphi=rac{2\pi e}{\lambda} heta_{\it L}, \qquad \Delta p_y=e t \Delta B_{\perp}$$

The magnetic phase shift relates to the magnetic flux quantum as,

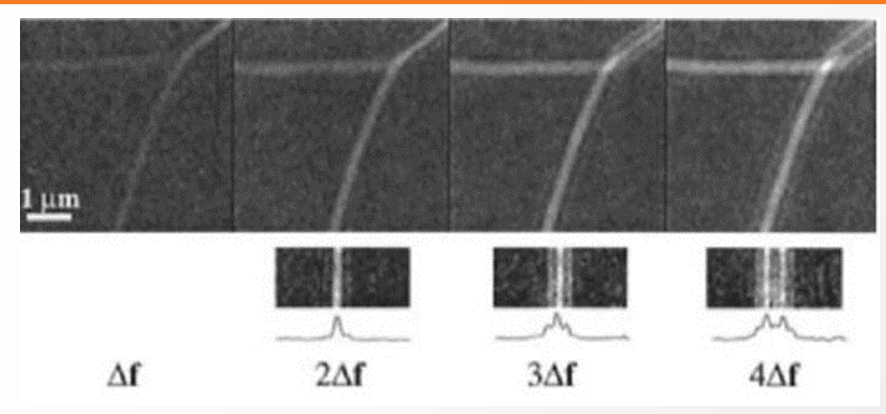
$$\Delta \varphi_m(r_\perp) = \frac{2\pi e}{h} \Phi_m(r_\perp) = \pi \frac{\Phi_m(r_\perp)}{\Phi_o}$$
, where $\Phi_o = \frac{h}{2e}$ is the flux quantum

Uncertainty principle states $\Delta p_y \Delta y \geq h$

$$\frac{\Delta y \Delta B_{\perp} t}{2} = \frac{\Delta \Phi}{2} \ge \frac{h}{2e} = \Phi_o$$

thomas.lagrange@epfl.ch • www.epfl.ch • lumes.epfl.ch • +41 (0)21 6935861

Quantum mechanical description of Lorentz TEM and fringe spacings in LTEM images



The angle (γ) between 2 sources on the image plane is,

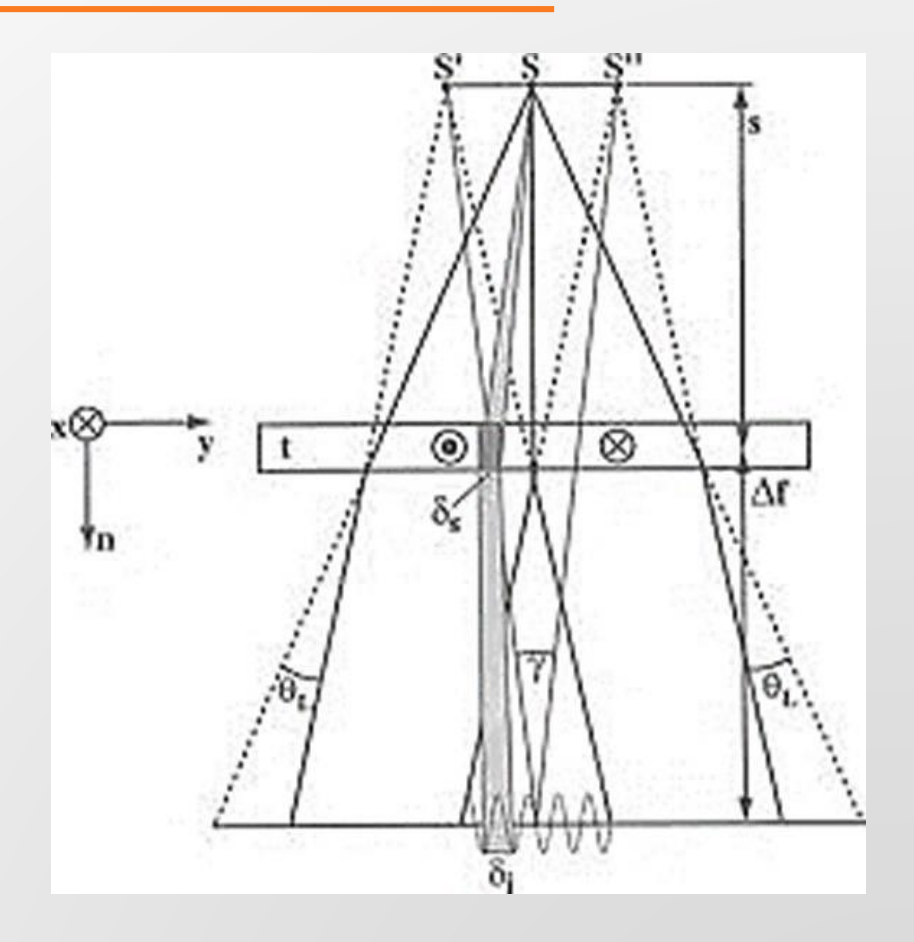
$$\gamma = 2s\theta_L/(s + \Delta f)$$

The fringe width can be described as,

$$\delta_i = \frac{\lambda}{\gamma} = \frac{h(s + \Delta f)}{2etsB_\perp}$$

The spatial region of the fringe at the sample plane is,

$$\delta_s = \delta_i \frac{s}{s + \Delta f} = -\frac{h}{2eB_{\perp}t} = \frac{\Phi_o}{tB_{\perp}}$$



$$\Phi_o = \delta_s \ tB_{\perp}$$

thomas.lagrange@epfl.ch • www.epfl.ch • lumes.epfl.ch • +41 (0)21 6935861